T.R.
GEBZE TECHNICAL UNIVERSITY
GRADUATE SCHOOL OF NATURAL AND APPLIED SCIENCES

DEVELOPMENT OF NOVEL ELECTRODE MATERIALS FOR Li-ION BATTERIES

MEHMET SINAN UYANIK
A THESIS SUBMITTED FOR THE DEGREE OF
MASTER OF SCIENCE
DEPARTMENT OF MECHANICAL ENGINEERING

GEBZE
2023

T.R.

GEBZE TECHNICAL UNIVERSITY

GRADUATE SCHOOL OF NATURAL AND APPLIED SCIENCES

DEVELOPMENT OF NOVEL ELECTRODE MATERIALS FOR Li-ION BATTERIES

MEHMET SINAN UYANIK

A THESIS SUBMITTED FOR THE DEGREE OF MASTER OF SCIENCE

DEPARTMENT OF MECHANICAL ENGINEERING

THESIS SUPERVISOR

ASST. PROF. DR. SEMIH AFYON

GEBZE

2023

T.C.
GEBZE TEKNİK ÜNİVERSİTESİ
FEN BİLİMLERİ ENSTİTÜSÜ

Li-ION BATARYALAR İÇİN YENİ ELEKTROT MALZEMELERİNİN GELİŞTİRİLMESİ

MEHMET SİNAN UYANIK

YÜKSEK LİSANS TEZİ
MAKİNE MÜHENDİSLİĞİ ANABİLİM DALI

DANIŞMANI
DR. ÖĞR. ÜYESİ SEMİH AFYON

GEBZE
2023

GEBZE TEKNİK ÜNİVERSİTESİ	**YÜKSEK LİSANS JÜRİ ONAY FORMU**

GTÜ Fen Bilimleri Enstitüsü Yönetim Kurulu'nun 12.01.2023 tarih ve 2023/03 sayılı kararıyla oluşturulan jüri tarafından 20.01.2023 tarihinde tez savunma sınavı yapılan Mehmet Sinan UYANIK'ın tez çalışması Makine Mühendisliği Anabilim Dalında YÜKSEK LİSANS tezi olarak kabul edilmiştir.

JÜRİ

ÜYE (TEZ DANIŞMANI)	: Dr. Öğr. Üyesi Semih AFYON
ÜYE	: Doç. Dr. Ali Murat SOYDAN
ÜYE	: Prof. Dr. Mustafa TUNCER

ONAY

Gebze Teknik Üniversitesi Fen Bilimleri Enstitüsü Yönetim Kurulu'nun ...…/……/…… tarih ve ……./…..... sayılı kararı.

İMZA/MÜHÜR

SUMMARY

In this work, a novel cathode material, V_2O_5-B_2O_3 glass composite with reduced graphite oxide, is proposed to improve electrochemical characteristics in comparison to V_2O_5 as a cathode material. Proposed material was synthesized with three different compositions, 80:20, 85:15 and 90:10 wt-% V_2O_5:B_2O_3. The characterization for the materials was done by using scanning electron microscope (SEM) and X-ray diffractions (XRD) methods. Coin cells employing the proposed materials as cathodes were assembled against metallic Li. The assembled batteries were cycled using varying current densities to investigate the electrochemical characteristics of the materials. Galvanostatic charge/discharge method was used to investigate the cycling performance of the materials. Varying current densities were used to investigate the rate capabilities of the materials. The 85:15 wt-% V_2O_5-B_2O_3 glass delivered the best electrochemical performance out of the three compositions examined. This material has the highest initial specific capacity (222 mAh/g), the highest capacity retention (64%) at 100^{th} cycle and recovers the majority of the initial specific capacity when cycled with various current densities. The electrochemical performance of V_2O_5-B_2O_3 glass composites was shown to be better in comparison to plain V_2O_5 as cathode material for Li-ion batteries.

Key Words: Lithium-ion Batteries, Cathode, Vanadium Pentoxide, Boron Oxide, Reduced Graphite Oxide.

ÖZET

Bu çalışmada, V_2O_5'in katot malzemesi olarak kullanımının elektrokimyasal özelliklerini iyileştirmek için, indirgenmiş grafit oksit katkılı V_2O_5-B_2O_3 cam kompozitleri önerilmiştir. Önerilen malzeme, 80:20, 85:15 ve 90:10 yüzde kütle oranlarında sentezlenmiştir. Sentezlenen malzemelerin karakterizasyonu için taramalı elektron mikroskobu (SEM) görüntüleri ve X-ışını kırınımı (XRD) yöntemleri kullanılmıştır. Önerilen malzemelerle hazırlanan katot kullanılarak düğme tipi hücreler hazırlanmıştır. Hazırlanan hücreler, farklı akım yoğunlukları kullanılarak çevrime tabi tutulmuş, özgün kapasite, çevrim performansı araştırılmıştır. İncelenen üç malzeme arasında 85:15 yüzde kütle oranına sahip V_2O_5-B_2O_3 camı en iyi elektrokimyasal performansı göstermiştir. Bu malzeme, en yüksek özgül kapasite değerine (222 mAh/g), 100 çevrim sonrasında en yüksek kapasite koruma oranına (64%) sahiptir. Çeşitli akım yoğunlukları kullanılarak çevrime tabi tutulduğunda, ilk özgül kapasitesinin yüksek kısmını korumuştur. Önerilen V_2O_5-B_2O_3 cam kompoziti ile V_2O_5 malzemesinin, lityum-iyon bataryalar için katot malzemesi olarak kullanımında gösterdiği elektrokimyasal performans başarılı bir şekilde iyileştirilmiştir.

Anahtar Kelimeler: Lityum-iyon Batarya, Katot, Vanadyum Pentoksit, Boron Oksit, İndirgenmiş Grafit Oksit.

ACKNOWLEDGEMENTS

I wish to express my sincerest gratitude to my advisor Asst. Prof. Semih Afyon for his guidance, his support, and teacher-student relationship he shared with me.

I wish to express my sincerest gratitude to Asst. Prof. Ali Murat Soydan for giving me the opportunity to pursue an academic career.

I want to thank and show my appreciation to my parents for their unwavering support throughout my educational career and for always striving to provide a brighter future for me.

I would also like to thank Ress. Assist. Hatice Öner for her direct and indirect support she gave me.

TABLE of CONTENTS

	Page
SUMMARY	v
ÖZET	vi
ACKNOWLEDGEMENTS	vii
TABLE of CONTENTS	viii
LIST of ABBREVIATIONS and ACRONYMS	x
LIST of FIGURES	xii
LIST of TABLES	xv
1. INTRODUCTION	1
2. BATTERIES	3
2.1. History of Batteries	3
2.2. Lithium-ion Batteries	4
2.2.1. Cathode Materials	8
2.2.2. Layered Oxide Cathode Materials	9
2.2.3. Spinel Oxide Cathode Materials	11
2.2.4. Olivine Cathode Materials	12
2.3. Anode Materials	13
2.4. Electrolytes	15
2.5. Separators	17
2.6. Vanadium-Based Cathode Materials	19
2.6.1. VO_2 Cathode Materials	19
2.6.2. LiV_3O_8 Cathode Materials	20
2.6.3. $Li_3V_2(PO_4)_3$ Cathode Materials	21
2.6.4. V_2O_5 Cathode Materials	23
3. EXPERIMENTAL	32
3.1. Chemicals Used in Experimental Work	33
3.2. Equipment Used in Experimental Work	33
3.3. Synthesis of Active Material	34
3.4. Preparation of Slurry	35
3.5. Assembly of Coin Cells	36

4. RESULTS AND DISCUSSION 38
4.1. 80:20 wt-% V_2O_5:B_2O_3 Glass 38
4.1.1. Electrochemical Tests 38
4.1.2. X-Ray Diffraction Patterns 40
4.1.3. Scanning Electron Microscope Images 41
4.2. 85:15 wt-% V_2O_5:B_2O_3 Glass 42
4.2.1. Electrochemical Tests 42
4.2.2. X-Ray Diffraction Patterns 44
4.2.3. Scanning Electron Microscope Images 45
4.3. 90:10 wt-% V_2O_5:B_2O_3 Glass 46
4.3.1. Electrochemical Tests 46
4.3.2. X-Ray Diffraction Patterns 48
4.3.3. Scanning Electron Microscope Images 49
5. CONCLUSION 51
6. DISCUSSION 53
7. FUTURE WORKS 54

REFERENCES 55
BIOGRAPHY 60

LIST of ABBREVIATIONS and ACRONYMS

Abbreviations and Acronyms		Explanations
α	:	Alpha
ε	:	Epsilon
δ	:	Delta
γ	:	Gamma
ω	:	Omega
θ	:	Theta
μ	:	Micro
°C	:	Degree celcius
cm		Centimeter
DEC	:	Diethly carbonate
DMC	:	Dimethly carbonate
EC	:	Ethylene carbonate
EV	:	Electric vehicle
ESS	:	Energy storage system
g	:	Gram
GPE	:	Gel polymer electrolyte
HDPE	:	High density polyethylene
kg	:	Kilogram
L	:	Liter
LIB		Lithium-ion battery
LVP	:	Lithium vanadium phosphate
LTO	:	Lithium-titanium-oxide
m^2	:	Square meter
mAh	:	Milliampere hour
MPM	:	Microporous polymer membranes
NASICON	:	Sodium superionic conductors
NCA	:	Nickel-cobalt-aluminum
nm	:	Nanometer

NMC	:	Nickel-manganese-cobalt
NMP	:	N-methyl-2-pyrrolid
O	:	Octahedral
P	:	Prismatic
PC	:	Propylene carbonate
PE	:	Polyethylene
PP	:	Polypropylene
ppm	:	Parts per million
PVDF	:	Polyvinylidene fluoride
rGO	:	Reduced graphite oxide
SEI	:	Solid electrolyte interface
SEM	:	Scanning electron microscope
T	:	Tetrahedral
V	:	Volt
Wh	:	Watt-hour
wt-%	:	Weight percentage
XRD	:	X-ray diffraction

LIST of FIGURES

Figure No:		Page:
2.1:	Volumetric and gravimetric energy density comparison for types of batteries.	5
2.2:	Working principle for a LIB.	7
2.3:	Schematics of different configurations for LIBs a) Cylindrical cell; b) Coin cell; c) Prismatic cell; d) Pouch cell.	7
2.4:	Schematic of the crystal structure of layered $LiCoO_2$. The cobalt and lithium ions alternately occupy layers of the octahedral sites, while the oxygen ions form tightly packed planes stacked in an ABCABC pattern.	10
2.5:	Lithium stoichiometric-layered transition-metal oxide phase diagrams: $LiCoO_2$, $LiNiO_2$, and $LiMnO_2$. The mentioned $LiNi_{1-x-y}Co_xMn_yO_2$ materials are represented by the places indicated by dots.	11
2.6:	Schematic for structure of spinel $LiMn_2O_4$.	12
2.7:	a) Olivine crystal structure. MO_6, PO_4, oxygen and lithium-ions are represented by brown, purple, red and greed, respectively. One-dimensional route for lithium-ions in olivine structure.	13
2.8:	Overcharge behavior of a shutdown separator.	17
2.9:	The crystallographic structure of VO_2(M) and VO_2(R).	20
2.10:	Schematic of formation of $Li_3V_2(PO_4)_3$/C nanocomposite.	22
2.11:	Schematic for the structures of bulk V_2O_5 and δ-V_2O_5.	24
2.12:	Schematic for structure of γ-V_2O_5.	25
2.13	a) SEM images for V_2O_5 prior to annealing. b-d) Following a one-hour thermal treatment in air at 500 °C, SEM pictures of V_2O_5.	26
2.14:	Schematic of nanosheet synthesis.	27
2.15:	Performance of pure and Sn-doped V_2O_5 during cycling at 500 mA/g current density.	28
2.16:	Performance of pure and Mn-doped V_2O_5 during cycling at 680 mA/g current density.	28
2.17:	Cycling performance of proposed 3 materials at 58.8 mA/g current density and at varying current density values between 1 C and 20 C.	29

2.18:	a) Galvanostatic charge-discharge curves of the V_2O_5/rGO (46 wt%) cathode material at 90 mA/g current density. b) Cycling performance of the material at 90 mA/g current density c) Cycling performance of the material at varying current densities between 190 to 5700 mA/g. d) Cycling performance of the material at 5700 mA/g current density.	30
2.19:	a) Cycling performance of RGO/V_2O_5–$LiBO_2$ glass composite at 50 and 100 mA/g current densities. b) Rate capability of the proposed material using 50, 100, 200 and 400 mA/g current density values.	31
3.1:	Flowchart of the study.	32
3.2:	Quenched V_2O_5-B_2O_3 glass.	35
3.3:	Aluminum coated with slurry.	36
3.4:	Schematic representation for assembly of a coin cell.	37
4.1:	Charge-discharge curves of 80:20 wt-% V_2O_5:B_2O_3 glass for first 10 cycles within the potential range of 1.5-4 V at 50 mA/g current density.	39
4.2:	Cycling performance of the 80:20 wt-% V2O5:B2O3 glass after 100 cycles within the potential range of 1.5-4 V at 50 mA/g current density.	39
4.3:	Cycling performance of the 80:20 wt-% V_2O_5:B_2O_3 glass material for varying current densities within the potential range of 1.5-4 V.	40
4.4:	XRD patterns of 80:20 wt-% V_2O_5:B_2O_3.	41
4.5:	SEM images of 80:20 wt-% V_2O_5:B_2O_3.	42
4.6:	Charge-discharge curves of 85:15 wt-% V_2O_5:B_2O_3 glass for first 10 cycles within the potential range of 1.5-4 V at 50 mA/g current density.	43
4.7:	Cycling performance of the 85:15 wt-% V_2O_5:B_2O_3 glass after 100 cycles within the potential range of 1.5-4 V at 50 mA/g current density.	43
4.8:	Cycling performance of the 85:15 wt-% V_2O_5:B_2O_3 glass material for varying current densities within the potential range of 1.5-4 V.	44
4.9:	XRD patterns of 85:15 wt-% V_2O_5:B_2O_3.	45
4.10:	SEM images of 85:15 wt-% V_2O_5:B_2O_3.	46
4.11:	Charge-discharge curves of 90:10 wt-% V_2O_5:B_2O_3 glass for first 10 cycles within the potential range of 1.5-4 V at 50 mA/g current density.	47
4.12:	Cycling performance of the 90:10 wt-% V_2O_5:B_2O_3 glass after 100 cycles within the potential range of 1.5-4 V at 50 mA/g current density.	47

4.13: Cycling performance of the 90:10 wt-% V_2O_5:B_2O_3 glass material for varying current densities within the potential range of 1.5-4 V. 48
4.14: XRD patterns of 90:10 wt-% V_2O_5:B_2O_3. 49
4.15: SEM images of 90:10 wt-% V_2O_5:B_2O_3. 50

LIST of TABLES

Table No:		Page:
2.1:	Advantages and disadvantages of LIBs.	5
2.2:	Electrochemical characteristics of common cathode materials.	9
2.3:	Theoretical capacity and potential of different anode materials.	15
3.1:	Chemicals used in experimental work.	33
3.2:	Equipment used in experimental work.	33
3.3:	Synthesized compositions and mass of the precursors used in synthesis.	34
3.4:	Materials and their mass used in preparation of slurry.	36

1. INTRODUCTION

Climate change, global warming and air pollution are some of the environmental issues that are posing an increasing danger to humanity. These issues are closely related to the usage of fossil fuel sources. Investigating feasible and environmentally-safe energy sources is essential due to the current energy problem. The major clean energy sources include but not limited to solar energy, hydropower, and wind energy. They all have an unstable and irregular character, which makes energy storage and using the stored energy more expensive and challenging. In the usage and storage of clean energy, rechargeable batteries are essential. Using clean energy sources for energy generation can be effectively stored using rechargeable batteries and delivered. Rechargeable batteries are also generally used to for powering electrical appliances and electric vehicles. The high performance need of electrical vehicles namely fast recharge time and high energy density rendered research in rechargeable batteries even more substantial.

Rechargeable batteries can be defined as electrochemical energy storage systems that carry out conversion between chemical energy and electrical energy reversibly. Lead-acid batteries, nickel-cadmium (Ni-Cd) batteries, nickel-metal hydride batteries (Ni-MeH), and lithium-ion batteries (LIB) are some of the extensively used rechargeable batteries. Considering the share of worldwide battery sales, compared to Ni-Cd (23%) batteries and Ni-MeH batteries (14%), LIBs accounted for the majority (63%) of those sales. Lead-acid batteries are only suitable for power the ignition, lights, and starting of vehicles. Power tools primarily utilize nickel-cadmium batteries because of their exceptional performance on high-power delivery [1].

Among rechargeable batteries, LIBs demonstrated highest volumetric and gravimetric energy densities while maintaining appropriate safety. Since the performance of LIBs is most severely controlled by cathodes, the most straightforward way to meet the rising demands and further boost the gravimetric energy density of LIBs is to improve the electrochemical characteristics of the cathode materials.

The aim of this thesis is enhancing the electrochemical characteristics of vanadium pentoxide (V_2O_5) as a cathode material. V_2O_5 was selected as a consequence of the high theoretical capacity of the material, but the practical performance is hindered by phase transitions resulting from lithium intercalation/de-intercalation and low electrical and ionic conductivity. The objective is to address these challenges and

strengthen the electrochemical characteristics of the V_2O_5. The proposed V_2O_5:B_2O_3 glass material with reduced graphite oxide (rGO) can solve these problems. The amorphous structure of the resulting material prevents occurrence of irreversible phase transformation, addition of rGO into the cathode increases electric conductivity and lithium diffusion rate of the material because of the intrinsic high conductivity of rGO and novel structures of the V_2O_5/rGO composites [2], [3].

2. BATTERIES

2.1. History of Batteries

Batteries can be defined as energy-storage systems that work by converting the chemically stored energy of the active material within them to electrical energy. Batteries have a long history dating back to the first century BC., to the Baghdad Battery. Since the Baghdad Battery predates the invention of electricity, Alessandro Volta is universally accepted as the inventor of the battery. Volta described his invention to Royal Society of London in a letter, today known as “Volta Pile”, in 1800. He used copper and zinc disks as electrodes separated by a cloth dipped in salt water. This device was later known as the first primary battery.

The next significant improvement in the history of batteries is “Daniel Cell”, developed in 1836. John Daniel used copper sulfate solution in a copper container. Another container with sulfuric acid and zinc electrode is placed into the copper container. The zinc electrode acted as the anode and the copper electrode as the cathode in this cell, which gave the standard potential of 1.1 V.

In 1866, Georges Leclanché invented the “Leclanché Cell”. This battery employs a glass jar filled with ammonium chloride which works as electrolyte, a carbon rod as positive electrode and a zinc rod which serves as the negative electrode in this battery. This battery gave the standard potential of 1,5 V.

The first secondary cell is invented by Gaston Planté in 1859. Planté employed two lead sheets in the form of spirals as electrodes. He used a porous cloth to separate the lead sheets, placed the system in glass jar filled with sulfuric acid. The “lead-acid battery” had the standard potential of 2 V, a battery consisting of 10 cells was demonstrated with the standard potential of 20 V.

At the end of 19th century, Swedish engineer Waldemar Jungner developed and patented the “nickel-cadmium battery”. Around the same period, Thomas Edison constructed and patented a battery known as the "nickel-iron battery." A combination of cadmium and iron powders served as the negative electrode in the nickel-cadmium battery, and nickel hydroxide served as the positive electrode. The nickel-iron battery used iron as the negative electrode. Both batteries employed their electrodes in a solution of potassium hydroxide and had the standard potential of 1,2 V. The rivalry between these two batteries laid the foundations of battery industry.

In 1912, G.N. Lewis made experimentations with lithium batteries. Lewis used lithium as anode and manganese dioxide as cathode in lithium batteries, but commercialization of lithium batteries was done in 1970. Following developments in the 1980s, in 1991 Sony commercialized LIBs.

2.2. Lithium-ion Batteries

The research regarding the lithium batteries began in 1970 and has continued to this day to investigate effective rechargeable electrical energy storage systems that may solve the poor volumetric and gravimetric energy density limitations of secondary batteries. M. Stanley Whittingham employed TiS_2 as a cathode material capable of effectively hosting and intercalating lithium ions in batteries. In 1980s, John B. Goodenough worked on $LiCoO_2$, which could be used as a substitute to metal sulfide for LIBs, that resulted in higher voltage values of ~3.5 - 4V. The higher voltage value resulted in higher energy density. These studies employed lithium metal as the anode, a material that is unsafe for battery applications because of explosivity and extreme reactivity of the lithium metal. In 1985, Akira Yoshino created the first LIB. In this battery, petroleum coke was used as anode along with $LiCoO_2$ as cathode. Akira Yoshino, M. Stanley Whittingham and John B. Goodenough, received the 2019 Nobel Prize in Chemistry for their research on LIBs [4].

Lithium is a soft, silvery-white colored alkali metal with the atomic number 3. It is the most electropositive and lightest metal. It also has the lowest reduction potential of any element. These properties of the lithium metal result in LIBS having high energy density and high cell potential.

The LIBs have peak energy densities of gravimetric energy value of 180 Wh/kg and volumetric energy value of 400 Wh/L. The high operating voltage, which is around 3.6 V, is connected to high energy density of lithium-ion batteries. Long lifetime, low rate of self-discharge, adaptable design, and not having memory effect are further benefits of LIBs [5], [6]. In Figure 2.1, energy density values of various secondary batteries can be seen.

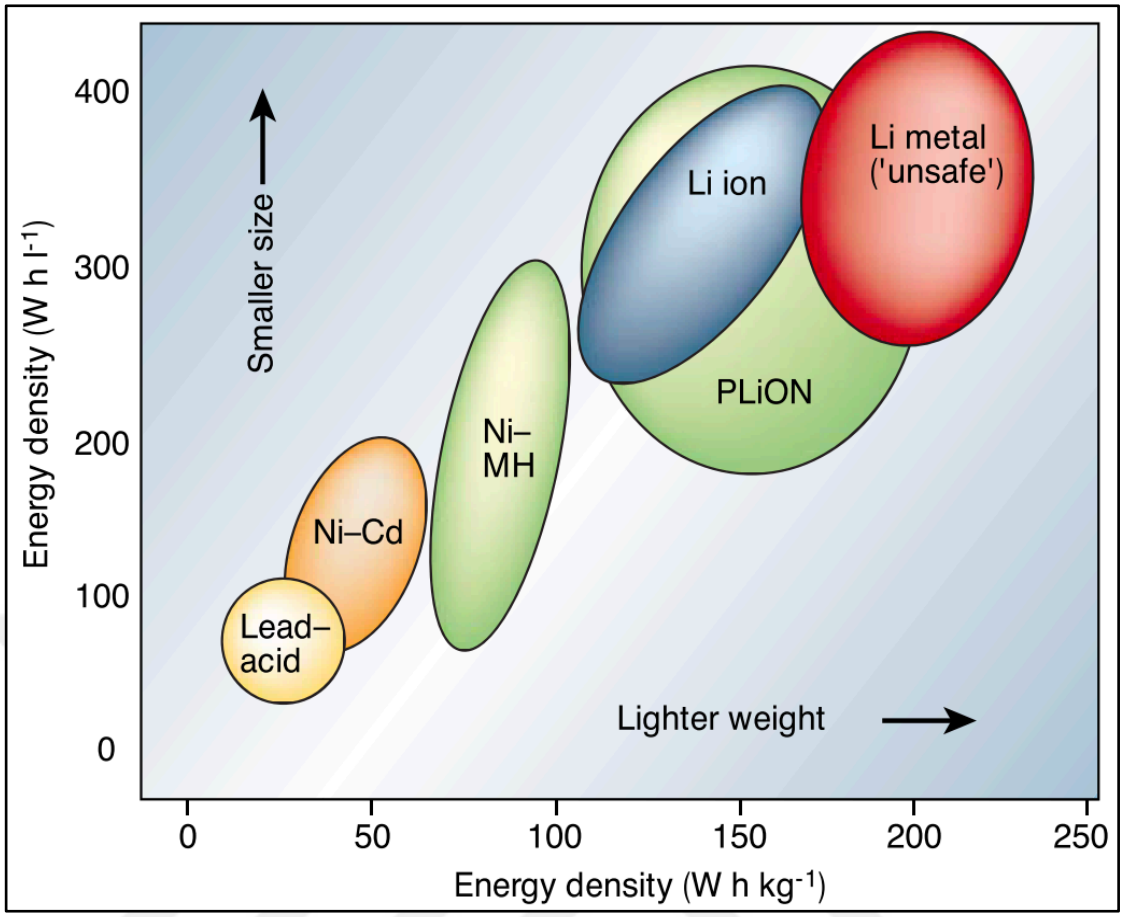

Figure 2.1: Volumetric and gravimetric energy density comparison for types of batteries.

Table 2.1: Advantages and disadvantages of LIBs.

Advantages of LIBs	**Disadvantages of LIBs**
High energy density	High cost of materials
Low self-discharge and long shell life	Requiring a protective circuit
Fast charge-discharge	Capacity loss due to overcharging
Being able to operate at a wide voltage range and a wide temperature range	High temperatures causing thermal decomposition
Long cycle life	
No memory effect	
Not needing maintenance	

These advantages rendered LIBs being useable in variety of fields such as consumer electronics, medical, automotive and consumer electronics.

The primary parts of a LIB are cathode (positive), anode (negative), electrolyte, and separator. Lithium containing metal oxides with layered structures, or materials with tunnel structures are typically employed as cathode materials. Anode materials can be categorized depending on the working mechanism; the insertion, conversion, and alloying types. The electrolyte must be an excellent ionic conductor as well as an electronic insulator. The majority of electrolytes are composed of a combination of two or more organic solvents and a solution of inorganic lithium salts. The separator serves to offer enough paths for lithium ions to travel while charging and discharging while preventing the negative and positive electrodes from short circuiting. Following their release by the cathode during charging, lithium ions are intercalated at the anode. During cell discharge, lithium ions are pulled out from anode and injected into the cathode. LIBs are also known as "rocking-chair batteries" because of how the way li-ions move between anode and cathode. Working principle of a LIB can be seen in the Figure 2.2 [7].

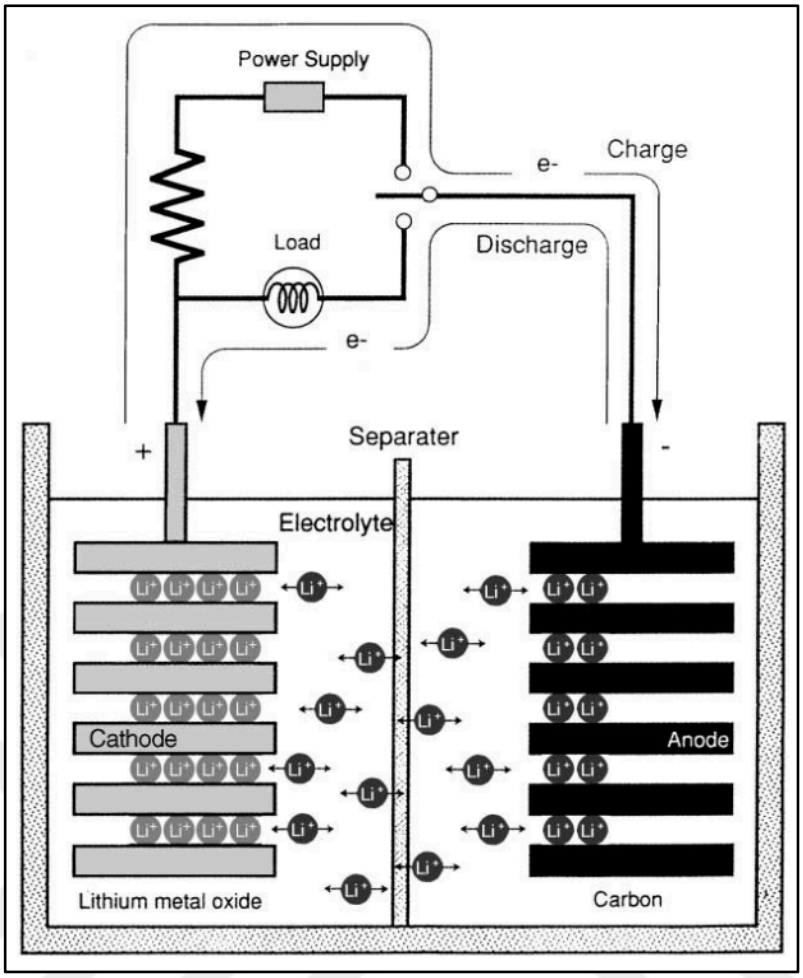

Figure 2.2: Working principle for a LIB.

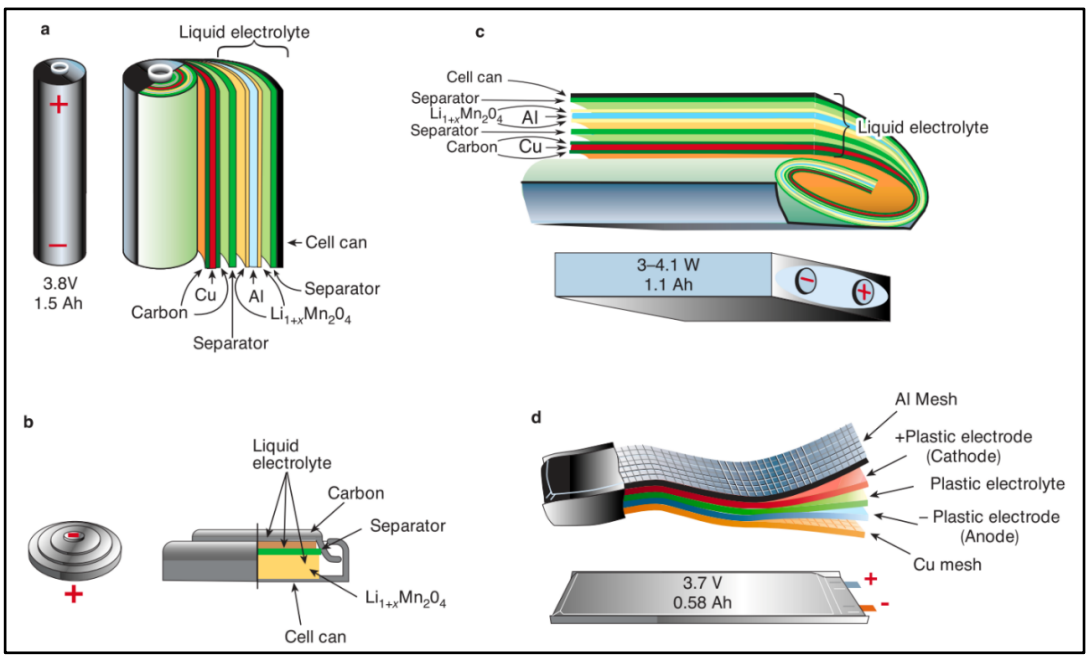

Figure 2.3: Schematics of different configurations for LIBs a) Cylindrical cell; b) Coin cell; c) Prismatic cell; d) Pouch cell.

There are four types of lithium-ion cell geometries: prismatic, cylindrical, coin, and pouch cell type. Because of their more flexible designs, pouch cell geometry is favored by major producers of smartphones and other portable devices. Nowadays, almost all the personal computers have transitioned to pouch cell geometry, allowing for slimmer, lighter laptops and tablets. Different types of cell geometries can be seen in the Figure 2.3 [8].

2.2.1. Cathode Materials

In lithium-ion batteries, the cathode serves as the positive electrode, acting as the positive pole during discharge and the negative pole during charge phase of the cycle. Cathode usually serves as the lithium source because the carbon electrode, which serves as the anode in LIBs, lacks lithium. Cathode materials can be categorized as layered oxides, spinel oxides and olivines. An ideal cathode material should have the following characteristics:

- An ideal cathode material must have high cell voltage and high specific capacity as both the specific capacity and operating voltage affect energy density. For high specific capacities, multiple lithium intercalations per formula are advantageous.
- An ideal cathode material should have high structural stability because the cycling performance of a cathode material is directly influenced by the structural stability of the material. Cathode materials must also maintain their stability while in contact with the electrolyte to ensure good cycle stability.
- An ideal cathode material should have high ionic and electric conductivity because li-ion and electron transport kinetics are primarily responsible for rate capability. The best options for cathode materials with excellent rate performance are nanostructured compounds with high electrical and ionic conductivities. The lengths that li-ions and electrons must travel during cycling are significantly decreased by nanoscale cathode materials. High rate performance translates into high power density.
- The progress regarding large-scale lithium-ion batteries has been severely constrained by the expensive and environmentally hazardous nature of commercial $LiCoO_2$ cathode materials. As a result, new cathode materials should be cheap and safe for the environment.

Comparison of the electrochemical characteristics and crystal structures of the most popular cathode materials is given in Table 2.2 [9].

Table 2.2: Electrochemical characteristics of common cathode materials.

	$LiCoO_2$	$LiMn_2O_4$	$LiFePO_4$	$LiNi_{0.8}Mn_{0.1}Co_{0.1}O_2$	$LiNi_{0.8}Co_{0.15}Al_{0.05}O_2$	$LiNi_{1/3}Mn_{1/3}Co_{1/3}O_2$
Structure	Layered	Spinel	Olivine	Layered	Layered	Layered
Theoretical Capacity ($mAhg^{-1}$)	274	148	170	279	279	275
Electrode Density (gcm^{-3})	3.9	3.2	2.3	3.4	3.4	3.46
Energy Density ($Whkg^{-1}$)	740	410	540	800	760	610
Operating Voltage (V)	3.9	4.0	3.4	3.8	3.8	3.8
Application	Mobile Devices Power Tools	Power Tools EVs ESSs	EVs ESSs	Power Tools EVs ESSs	Power Tools EVs ESSs	Power Tools EVs ESSs

2.2.2. Layered Oxide Cathode Materials

The general formula for the structure of crystalline layered oxides is A_xMO_2. Oxygen atoms in the crystal formations are tightly packed, transition metal, shown as M and the alkali, shown as A, cations fill the interstitial positions in alternate layers. MO_2 sheets, which consist of MO_6 octahedra sharing edges, are produced as a consequence of M cation-filled layers. The A cations can intercalate and de-intercalate to the layers amid the sheets of MO_2 and can fill and prismatic (P), octahedral (O), tetrahedral (T), sites [10].

Layered $LiCoO_2$ is the first oxide cathode that has been studied. Goodenough noted that $LiCoO_2$ had a structure akin to layered dichalcogenides and demonstrated electrochemical extraction of lithium. The oxygens in $LiCoO_2$ are arranged in a close-packed cubic α-$NaFeO_2$ configuration. When the lithium is completely removed, the layers of oxygen reposition to give themselves a compact and hexagonal structure. As a result of approximately 0.5 Li/Co being cycled without initiating irreversible structural changes in $LiCoO_2$, the theoretical capacity of the material is 130 mAh/g.

Phase shifts that result in slow response rates and the electrode's poor stability at low lithium levels can both be attributed to this phenomenon [11]-[13].

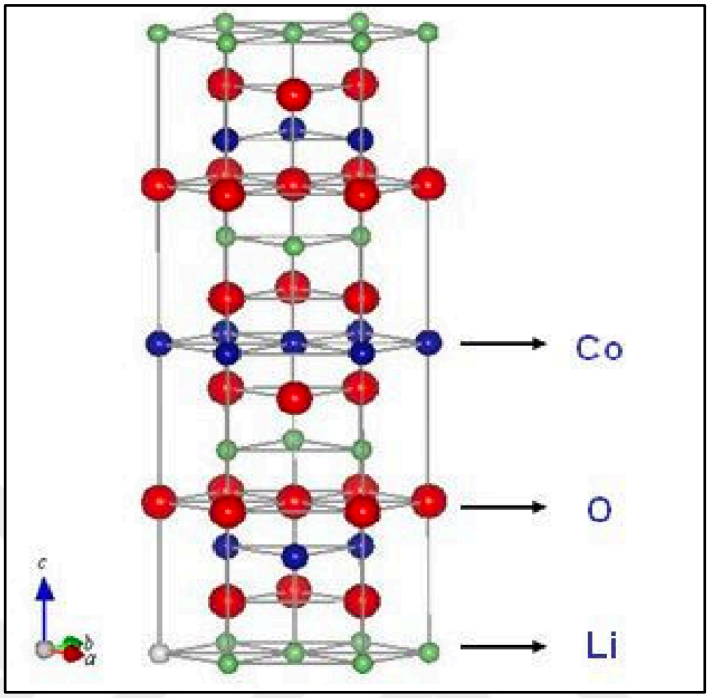

Figure 2.4: Schematic of the crystal structure of layered $LiCoO_2$. The cobalt and lithium ions alternately occupy layers of the octahedral sites, while the oxygen ions form tightly packed planes stacked in an ABCABC pattern.

$LiNiO_2$, which shares the same structure as $LiCoO_2$, has not been researched extensively due to the material's poor thermal stability and instability at low lithium concentrations.

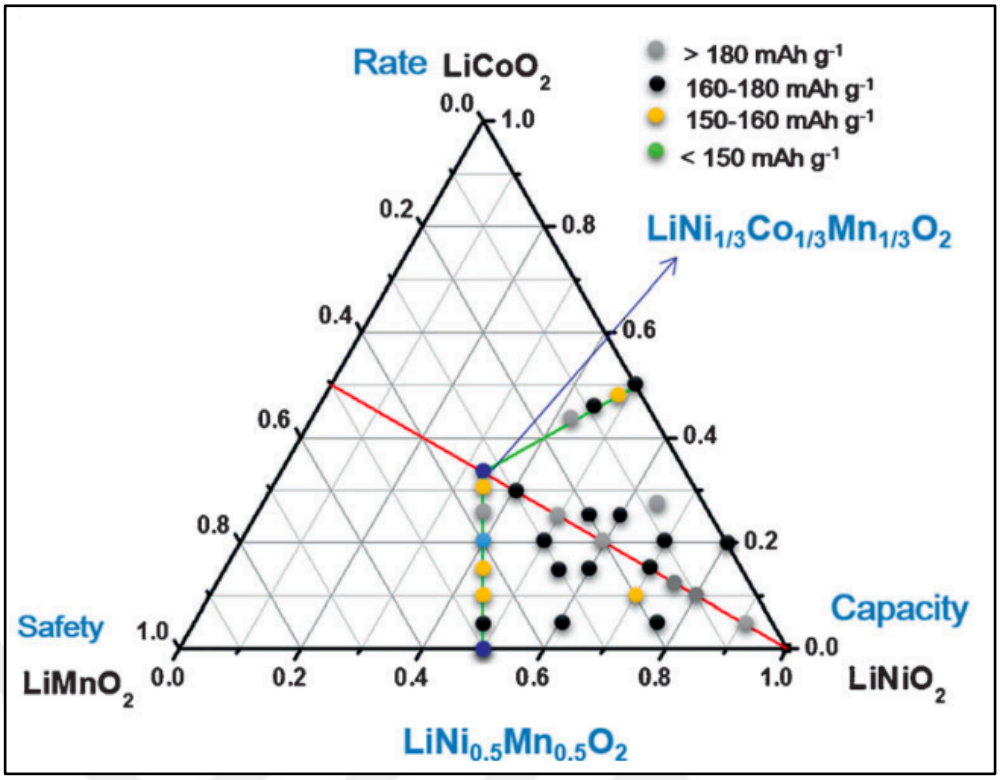

Figure 2.5: Lithium stoichiometric-layered transition-metal oxide phase diagrams: $LiCoO_2$, $LiNiO_2$, and $LiMnO_2$. The mentioned $LiNi_{1-x-y}Co_xMn_yO_2$ materials are represented by the places indicated by dots.

Recently cobalt has been replaced with Mn, Ni, and Al to create $LiNi_{1-y-z}Mn_yCo_zO_2$ and $LiNi_{1-x-y}Co_xAl_yO_2$ due to high cost and low capacity of $LiCoO_2$. Each transition-metal ion in NMC (Nickel-Manganese-Cobalt) and NCA (Nickel-Cobalt-Aluminum) has unique benefits and drawbacks. Improving the relative proportion of Ni in the NMC and NCA cathodes' composition is a straightforward way for increasing their capacity. Increasing the Ni content in NCM cathodes results in a decline in cycling stability along with thermal performance. Due to their high Ni content, nickel enriched NCA cathodes are anticipated to have capacity fading and thermal issues similar to NCM cathodes [14]-[16].

2.2.3. Spinel Oxide Cathode Materials

The general formula for spinel structure is AB_2O_4 and $LiMn_2O_4$ is the first reported material with this structure. In spinel $LiMn_2O_4$ with spinel structure, octahedral sites are occupied by manganese and tetrahedral sites are occupied by lithium. Instead of planes as in the α-$NaFeO_2$ configuration (e.g., LCO), the routes for

lithiation and de-lithiation in this case are channels working in three dimensions. $LiMn_2O_4$ has a lesser capacity but is cheaper and safer than $LiCoO_2$. $LiMn_2O_4$ also undergoes phase transformations during cycling. To overcome the shortcomings of the material, $LiMn_2O_4$ has been combined with alternative transition metals, like nickel, iron, cobalt. The inclusion of nickel lowers the electrical conductivity and lattice parameter of the structure. As the manganese concentration increases, the capacity increases and $LiNi_{0.5}Mn_{1.5}O_4$ could be obtained using 1:3 Ni:Mn ratio. $LiNi_{0.5}Mn_{1.5}O_4$ could be seen as the improved version of the $LiMn_2O_4$ because of the higher specific capacity of the material [17]-[19].

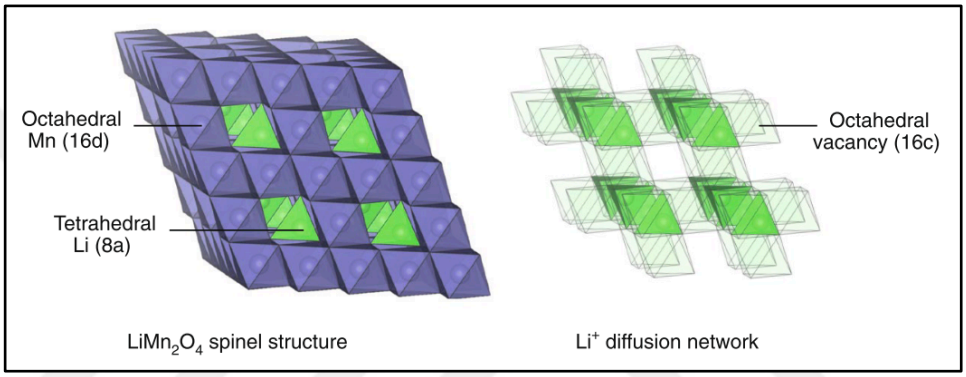

Figure 2.6: Schematic for structure of spinel $LiMn_2O_4$.

2.2.4. Olivine Cathode Materials

The general formula for olivine is M_2XO_4, with M atoms partially occupying octahedral positions and X atoms occupying 1/8 of a tetrahedral space in a hexagonally close-packed oxygen matrix. Fe, Mn, Co, and Ni are transition metals that are used to create the $LiMPO_4$ with a controlled olivine structure.

Two octahedra LiO_6 and one tetrahedron of PO_4 links to octahedron of MO_6 in the olivine structure. Due to the detachment of tetrahedra polyanions of LiO_6 and octahedra of MO_6, ion diffusion inside the crystal occurs along the 1D pathway (010), which inhibits rapid ion extraction and insertion [20].

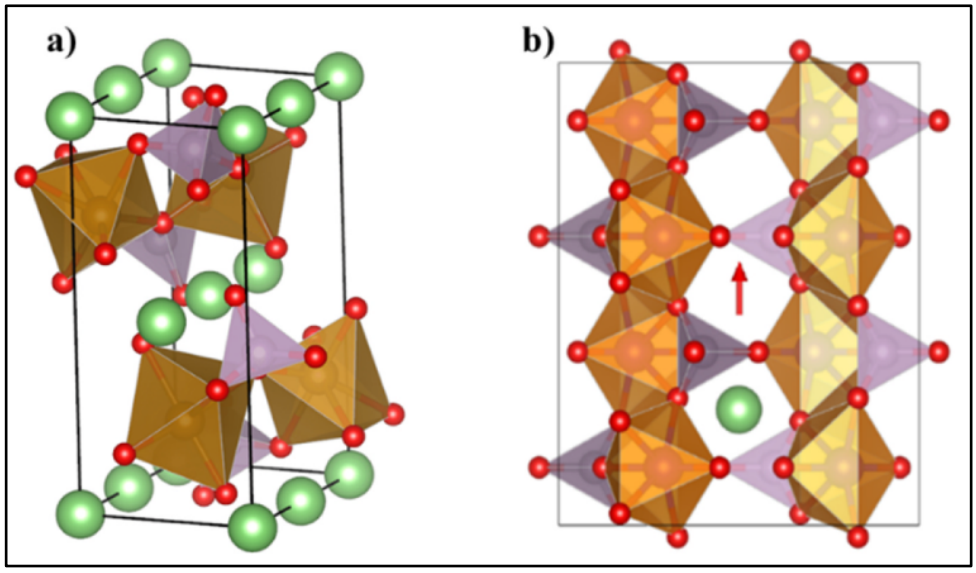

Figure 2.7: a) Olivine crystal structure. MO_6, PO_4, oxygen and lithium-ions are represented by brown, purple, red and greed, respectively. One-dimensional route for lithium-ions in olivine structure.

The most common cathode material with olivine structure is $LiFePO_4$. This cathode material has a theoretical capacity value of 170 mAh/g. As a result of olivine structure, which allows lithium ions being extracted and inserted completely during the lithiation and de-lithiation mechanisms, the material has a high cycle life.

The advantages OF cathode materials with olivine structure are high operating voltage ranges, high energy density and capacity, great cycling and safety. The downsides of the cathode materials are low cycle stability and rate performance. In literature, reducing the particle size, doping with additional D block elements, and coating with carbon, has shown that the material can be improved [21], [22].

2.3. Anode Materials

One of the most common materials utilized as an anode in LIBs is graphite. The insertion and extraction of li-ions in and out of the layered structure of graphite provides the basis for its electrochemical activity. The rate capability of LIBs using graphite as the negative electrode and a suitable positive electrode is constrained by the slow li-ion diffusion being slow inside of the electrode materials. Graphite undergoes lithium-ion insertion at a voltage less than 1 V when working against lithium. When the electrolyte is reduced at such low potentials, a solid electrolyte interface (SEI) layer forms on the surface of the graphite during the initial cycles. Since

SEI inhibits additional electrolyte reaction at the electrode surface, its production is necessary for the functioning of graphite electrodes. The SEI layer, however, impairs intercalation and extraction of lithium ions during following cycles, resulting in subpar cycling performance of the battery. Additionally, permanent capacity loss occurs during the initial cycles of SEI formation. Poor energy density and safety concerns associated with lithium deposition are drawbacks of the graphite anode [23].

The drawbacks of the graphite anode can be overcome by utilizing an electrochemical redox pair that intercalates and de-intercalates lithium ions at a higher voltage This need is fulfilled by $Li_4Ti_5O_{12}$ (LTO), with the Ti^{4+}/Ti^{3+} redox couple operating at around 1.55 V when working against lithium. The cycle life and rate capacity of LIBs can be increased by using LTO as the anode. The application of LTO in nanostructured forms can further enhance its performance. Doping the material with the proper anions or cations can increase the electrical conductivity of the material, which raises the power capacity of the LTO anode. Another effective way to increase the electrical conductivity of the material is by coating it with carbon [24].

As a consequence of safety features and high specific capacity provided by alloy anodes, they are a considered as a promising candidate. Theoretically, alloy anodes have specific capacities that are greater than graphite anodes and $Li_4Ti_5O_{12}$. Even after taking into account the whole volume expansion of lithiated products, alloy anodes still have charge densities that are greater than those of graphite and $Li_4Ti_5O_{12}$. The operating potential of alloy anodes when working against lithium is their second advantage. The major constraint in using alloy anodes is the extreme volume change they face during the insertion and extraction of lithium, which frequently results in poor cycle stability and deformation of the active alloy particles [25].

Capacity values and average potential of the materials when working against lithium of the most common anode materials can be seen in Table 2.3.

Table 2.3: Theoretical capacity and potential of different anode materials.

Material	Capacity (mAh/g)	Average V vs Li.
Graphite	300-340	0,15
33% Silicon	300	0,3
$Li_4Ti_5O_{12}$	160	1,55
Mg_2Si	410	0,35
SiB_3	440	0,3
Sn_2BPO_6	450	0,5
SnO_2	500	0,4
Sb	560	0,95
Sn glass	650	0,4
SiO	850	0,3

2.4. Electrolytes

The majority of electrolytes are salts dissolved in aqueous or non-aqueous solvents, which are liquid over the operational temperature ranges. In lithium-ion batteries aqueous electrolytes cannot be used because voltage of these batteries is always higher than 3 V; and that voltage value would decompose the electrolyte. Electrolyte should be inert toward the electrodes; it must have high ionic conductivity but a poor electronic conductivity. For the reactions to proceed and the electrons to continue flowing in the external circuit, the ions in the electrolyte migrate to balance these charges. Lithium-ion mobility and the quantity of mobile ions are inversely correlated with the ionic conductivity. Despite having high dielectric constants, carbonates such as ethylene carbonate (EC) and propylene carbonate (PC) have immense viscosities because of interactions between molecules that cause deviations in the electric charge of the molecules. For the lithium ions to travel more easily, lower viscosity is preferable. However, even while the viscosity and dielectric constant values of chain-like esters like dimethyl carbonate (DMC) and diethyl carbonate (DEC) are fairly low, they do not provide as much of a barrier to the movement of lithium ions inside the molecules. Additionally, when the dielectric constant increases, the coulombic force between a molecule's positive and negative sites increases,

causing a substantial amount of ionic dissociation in the nearby molecule. Mixing two or more solvents, such as EC and DMC, is a standard method to get the appropriate characteristics needed for high performance batteries [8].

Because of the economic viability, additives to electrolytes have been investigated thoroughly. It is more practical and cost-effective to enhance battery performance by adding modest amounts of components to the electrolyte without changing the composition of the electrolyte. The cyclability and cycle life of LIBs are greatly increased by the inclusion of an additive, which is present in an electrolyte at a maximum concentration of 5% by weight or volume [26]. By using additives, a plethora of advantages can be achieved, such as:

- Promote SEI development on the surface of graphite
- Decrease gas production and irreversible capacity for SEI formation
- Enhance the electrolyte's physical characteristics, including ionic conductivity, viscosity.
- Reduce the flammability of organic electrolytes, enhance overcharge tolerance, or provide overcharge protection
- Improve thermal stability of $LiPF_6$ against electrolyte solvents and safeguard cathode material from overcharging and degradation.

A polymer electrolyte is a membrane having transport characteristics similar to those of conventional liquid ionic solutions. Polymer electrolytes have uses in other electrochemical devices, such as super capacitors and electrochromic devices, in addition to lithium batteries. These polymer electrolytes are superior to their liquid counterparts in several ways. The membrane serves as both a separator and an electrolyte. The battery industry finds the idea interesting since polymer electrolyte lithium-ion batteries are predicted to be less expensive and easier to seal than their liquid electrolyte competitors. The advantages of polymer electrolytes are the elimination of internal shorting, avoidance of electrolyte leakage, and non-explosive reaction by-products near electrode surface [27], [28].

2.5. Separators

Separators are installed amid cathode and anode to avoid their connection, allowing free ionic movement, and preventing electrical short circuits. The most important characteristics of separators are electrical conductivity being minimal, ionic flow being high, chemical stability being high versus electrolytes, mechanical and dimensional stability being high, along with great wettability. Separator must not allow flow of ions and avoid thermal runaway in case of the short-circuiting of the battery. This is feat is achieved by melting the separator entirely or in portions, plugging the pores, and completely obstructing the passage of ions between the electrodes. As a result, the battery reactions are minimized [29], [30].

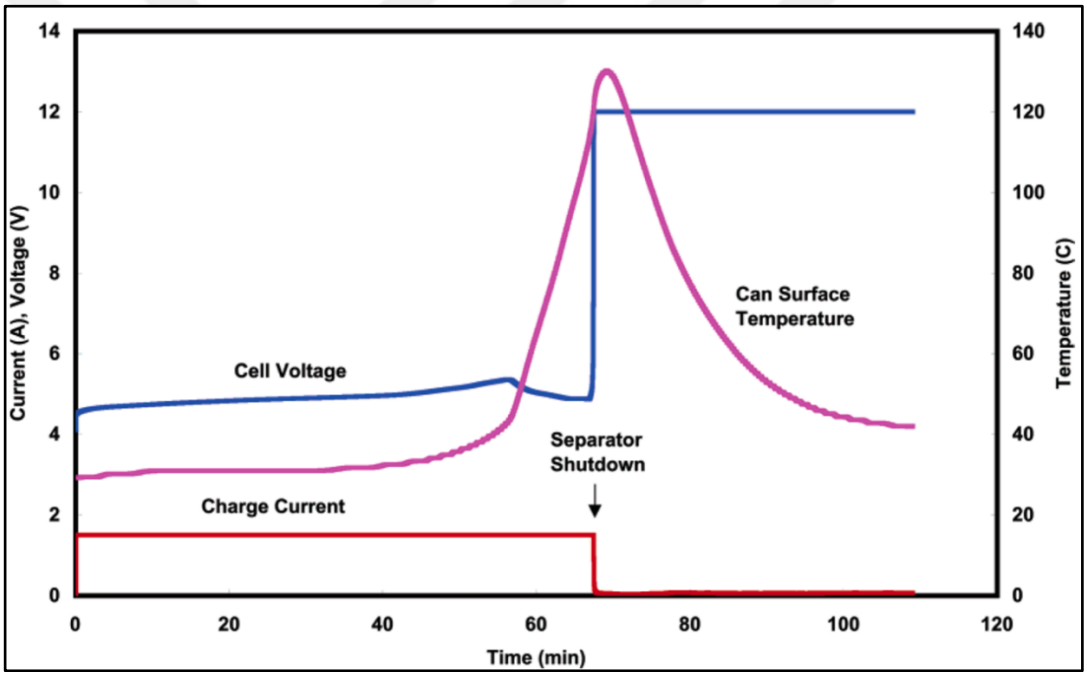

Figure 2.8: Overcharge behavior of a shutdown separator.

The three main categories of battery separators are determined by their structure and composition: Microporous polymer membranes (MPMs), non-woven fabric mats, and organic composite membranes. These three different separation methods are distinguished, respectively, by their leanness, immense porosity, and exceptional thermal dependability. Polyolefin materials and their blends are the basis of most MPMs used in LIBs. There are two different ways to make MPMs: dry and wet process. These approaches use an exclusion stage to create lean films and at the very

least one orientation processes to provide porosity and boost tensile strength. The majority of microporous polyolefin membranes have an moderate pore size less than 1 μm and are thinner than 50 μm. Decreasing the thickness can make mechanical penetration more dangerous. The characteristics of polyolefin materials affect the thermal properties of the membranes. For example, mechanical integrity of high density polyethylene (HDPE) membranes are lost above their melting point, which is 135°C. Membranes formed by laminating layers of polyethylene (PE), polypropylene (PP) are mechanically stable up to the melting point of PP, which is the 165 °C.

A non-woven separator is a fibrous mat produced via binding plentiful fibers in conjunction chemically, physically, or mechanically. The fibers of non-woven separators have been produced using both natural (celluloses and cellulose derivatives) and synthetic materials. Resin bonding and thermoplastic fiber bonding are the two main bonding techniques for battery separators. Immense porosity and huge pore size are characteristics of non-woven separators (20–50 μm). The labyrinth-like pores that characterize their architectures are particularly useful in reducing the occurrence of dendritic lithium in rechargeable lithium metal and LIBs. Non-woven mats are mostly utilized in lithium-ion batteries as the structural foundation for gel polymer electrolyte (GPE) batteries. The GPE can be easily soaked into non-woven separators and infuse the rough facet because of their immense porosity and huge pore size. Thus, the GPE offers the essential ionic conductivity between the electrodes while the non-woven nature acts as the mechanical support.

A porous mat comprised of extremely tiny inorganic particles joined together with a minimal quantity of binder is an inorganic composite separator. As a result of the strong hydrophilicity and immense surface of the tiny inorganic particles, such separators display outstanding wettability with all non-aqueous liquid electrolytes. These separators have exceptional thermal stability and demonstrate no shrinkage at high temperatures. While the immense thermal stability provides the batteries with excellent temperature tolerance, which is crucial for large-scale LIBs, the exceptional wettability facilitates the use of liquid electrolytes with high PC and EC concentrations, which is particularly beneficial to enhancing the cyclability of Li-ion batteries at high temperatures.

2.6. Vanadium-Based Cathode Materials

Vanadium is a hard, silvery-grey transition metal with the atomic number 23. The oxidation states of the element are 2+, 3+, 4+ and 5+ with the corresponding oxides of VO, V_2O_3, VO_2, and V_2O_5, respectively. In addition to these oxides, vanadium also has some oxides with mixed valence states including V_6O_{13}, V_4O_9, and V_3O_7. Vanadium-based cathode materials are a favorable candidate for LIBs because of the high working voltage, high theoretical capacity, and high energy density of the material. Vanadium-based oxides have received the most attention among vanadium-based cathode materials due to their high specific capacity. However, the cycle life and rate performance of conventional vanadium-based oxide electrodes cannot match the requirements due to their inherently weak conductivity [31].

2.6.1. VO_2 Cathode Materials

At around 68°C, A reversible metal to semiconductor phase change occurs in VO_2. This transition occurs alongside a structural change in symmetry from monoclinic ($P2_1/c$, M1 phase) to tetragonal (P42/mnm, R phase). In contrast to the V-V chain of VO_2(M), which is serrated and has lattice spacings of 0.313 and 0.266 nm, respectively, the V-V chain of VO_2(R) is linear along the c_R axis. The structure of VO_2(M) and VO_2(R) can be seen in Figure 2.9 [31], [32].

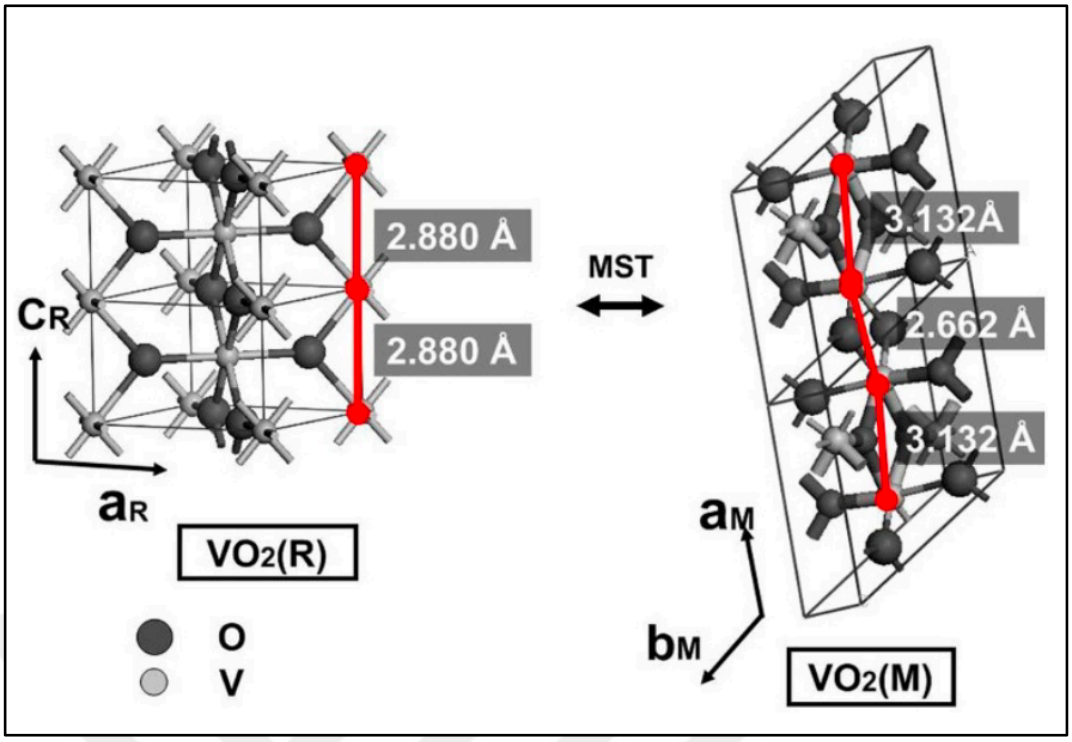

Figure 2.9: The crystallographic structure of VO_2(M) and VO_2(R).

Due to its quick lithium-ion intercalation and deintercalation in double layers of V_4O_{10} structure for lithium batteries, VO_2(B) is of more appeal. However, rapid capacity fading, and self-aggregation of the material severely limit the ability to be used on a broad scale [33].

In literature, research has been done for improving the electrochemical performance of the material. Various morphologies such as nanobelts, nanorods, nanowires have been investigated. Niu et al. constructed hollow microspheres with a radially expanding core made of VO_2 nanowires. They reported the use of hollow microspheres in high-rate, long-life lithium batteries are very promising, and the same morphology could also be used in other cathode materials [34].

Yang et al. reported the VO_2(B) doped with 3% nickel have a specific discharge capacity value of 163 mAh/g, which is almost 70% higher than pure VO_2(B) [35].

2.6.2. LiV_3O_8 Cathode Materials

LiV_3O_8 is a highly effective intercalation host because it contains two fundamental structural components, VO_6 octahedra and VO_5 distorted trigonal bipyramids, which create two distinct lithium-ion sites, namely octahedral and

tetrahedral. A zigzag double ribbon is created by the VO_6 octahedra, while a similar ribbon is created by the VO_5 bipyramids. A V-O layer is created between the two ribbons by corner-sharing oxygen ions [36]. Three lithium-ions can be intercalated into the material, which results in theoretical capacity value of the 280 mAh/g. To improve the electrochemical performance of the material, controlling the homogeneity, controlling the particle size, cation substitution, surface coating and doping has been investigated [37].

Mei et al. used VO_2(B) nanosheets to produce LiV_3O_8 nanorods. The LiV_3O_8 nanorods have been reported to have significantly improved reversible capacities, high-rate capability, and long-term cycling stability. The synthesized cathode material can be cycled at 2000 mA/g with 161 mAh/g capacity and 3000 mA/g with 158 mAh/g. Between 300 and 500 cycles, a low capacity loss of 0.037% and 0.031% per cycle has been reported [38].

Song et al. investigated Mo-doped LiV_3O_8 nanosheets assembled from nanorods. They synthesized the material via a hydrothermal process using $LiOH{\cdot}H_2O$, V_2O_5 and $(NH_4)_6Mo_7O_{24}$, then thermal annealing. Compared to the standard LiV_3O_8, synthesized material has better cyclic stability and rate capability. The maximum discharge capacity of 269 mAh/g and is achieved. After 100 cycles, 205.9 mAh/g at a current density of 300 mA/g is achieved [39].

2.6.3. $Li_3V_2(PO_4)_3$ Cathode Materials

There are two distinct forms of $Li_3V_2(PO_4)_3$ (LVP), rhombohedral (NASICON) and mono-clinic phase. High ionic conductivity is a benefit of the rhombohedral structure, which permits broad substitution on the octahedral and tetrahedral sites [40]. Monocline LVP is a better candidate as a cathode material because of the higher thermodynamical stability of the material. LVP is a promising cathode material for LIB applications due to a number of its benefits such as high energy density, high theoretical capacity caused by intercalating three lithium-ions (197 mAh/g) and operating voltage (up to 4.6 V), relatively good lithium-ion mobility, excellent thermal and cycle stability, and high safety performance [37]. The downside of the material is weak intrinsic electrical conductivity, leading to slow lithium-ion extraction/insertion notably for the third lithium, presenting a significant barrier that restricts practical uses of the material. Significant advances have been noted in the

literature when LVP bulk materials are tailored to reach a nano-level. Surface coating, doping, and preparing composite materials are other methods for increasing the electrochemical performance of the material [41]

To overcome the low electrical conductivity problem, conductive coating has been investigated. Fei et al. reported a significant enhancement on electrochemical performance by controlling the particle size and conductive coating. They synthesized a material by integrating core-shell $Li_3V_2(PO_4)_3$/C nanospheres at approximately 50 nm into a porous carbon framework. The resulting material had 130 mAh/g initial discharge capacity, with 90% capacity retention at 1200 cycles [42].

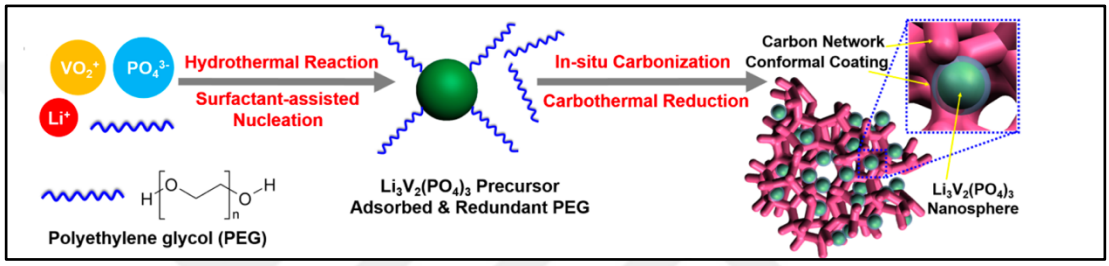

Figure 2.10: Schematic of formation of $Li_3V_2(PO_4)_3$/C nanocomposite.

In literature, it has been shown that increasing the reaction kinetics would also benefit the electrochemical performance of a cathode material. Zeng et al. reported a significant increase in electrochemical performance by anion/cation co-substitution, and carbon coating. They synthesized $Li_3V_{1.95}Mg_{0.05}(PO_4)_{2.9}Cl_{0.1}$, a material with a thin carbon coating partially occupied by Mg^{2+} and Cl^-, by using the sol-gel method. Resulting LVP had 130.1 mAh/g initial capacity and 80% capacity retention at 2C current rate after 650 cycles. They concluded the increase in performance was caused by shorter ion and electron transport route and faster reaction kinetics [43].

Zhong et al. synthesized $2LiVPO_4F \cdot Li_3V_2(PO_4)_3$/C composite cathode material by sol-gel method. They reported that the synthesized composite material had better electrochemical performance than $LiVPO_4F$/C and $Li_3V_2(PO_4)_3$/C. They reported 143.4 mAh/g at 0.1C, 141.6 mAh/g at 0.2C, 133.2 mAh/g at 0.5 C, 124.1 mAh/g at 1 C and 117.6 mAh/g 2 C rate. They also reported that when the discharge rate drops back to 0.1 C, practically all the discharge capacity could be recovered [44].

2.6.4. V_2O_5 Cathode Materials

V_2O_5 is a layered oxide cathode material studied extensively due to its high electrochemical activity, high energy density, and higher capacity compared to traditional cathode materials like $LiCoO_2$ and $LiFePO_4$ [45].

Reversible and irreversible phase changes occur when lithium is intercalated into V_2O_5. α-, ε and δ phases are reversible phases. These phase transformations depend on the amount of lithium intercalated into the structure. α-$Li_xV_2O_5$ occurs when $x<0.01$, ε-$Li_xV_2O_5$ occurs when lithium amount is between 0.35 and 0.7, and δ-$Li_xV_2O_5$ occurs when lithium amount equals to 1. Although there is a greater puckering of the layers, the framework of the α-$Li_xV_2O_5$ and ε-$Li_xV_2O_5$ phases matches that of the unintercalated phase in a very similar way. The α and ε phase transformations are completely reversible. Compared to the α and ε phases, the layers of the δ phase are more puckered. Additionally, there is a slight shift between layers in δ phase. As no strong vanadium-oxygen bonds are broken during shifting of layers, this phase transformation is also completely reversible. Reversible cycling of these phases is possible with 147 mAh/g theoretical capacity value [46], [47].

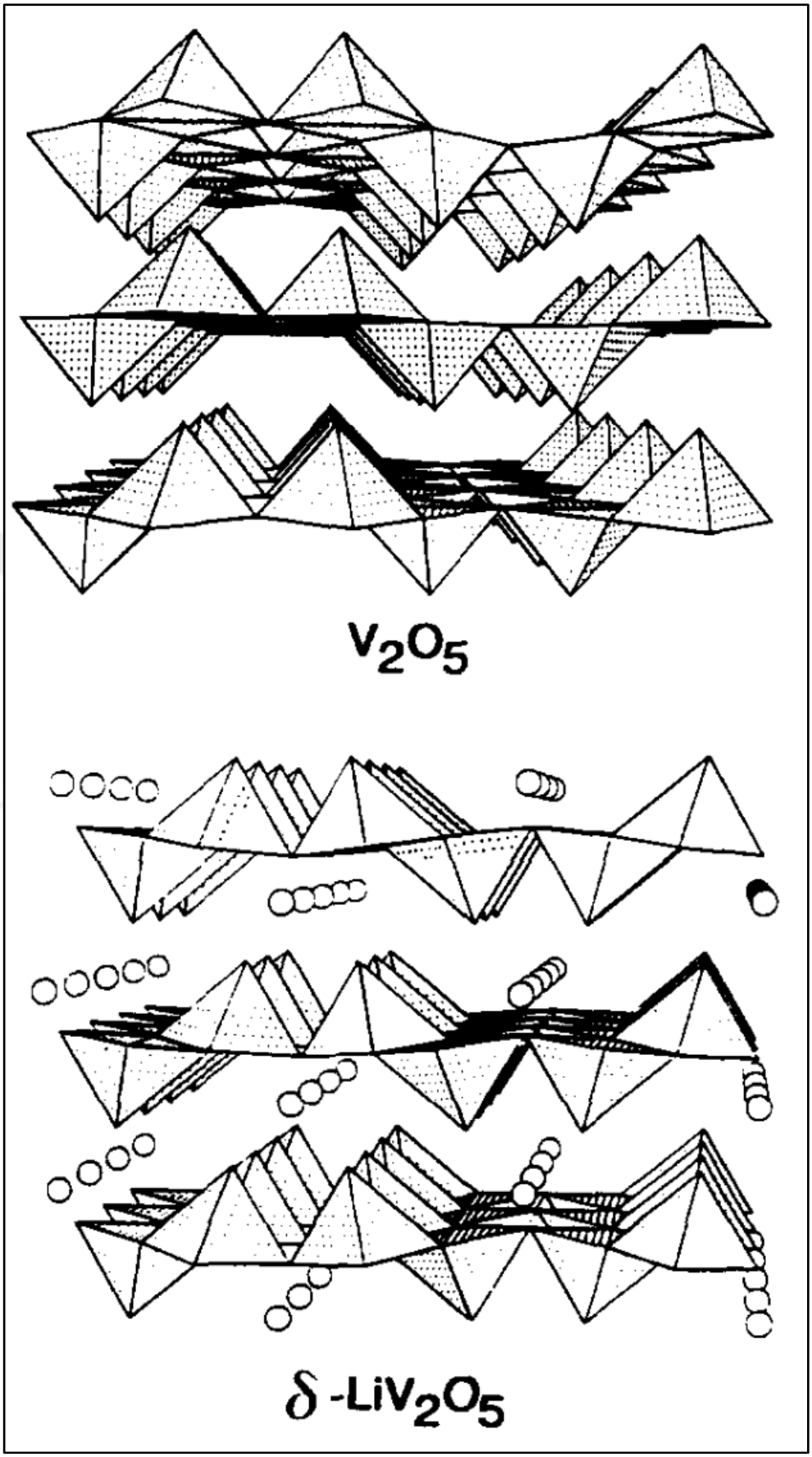

Figure 2.11: Schematic for the structures of bulk V_2O_5 and δ-V_2O_5.

The first irreversible phase transformation, γ-$Li_xV_2O_5$, occurs when 1<x<2. Cycling of this phase is possible without occurrence of structural alterations within the spectrum of 0<x<2, with a theoretical capacity value of 294 mAh/g.

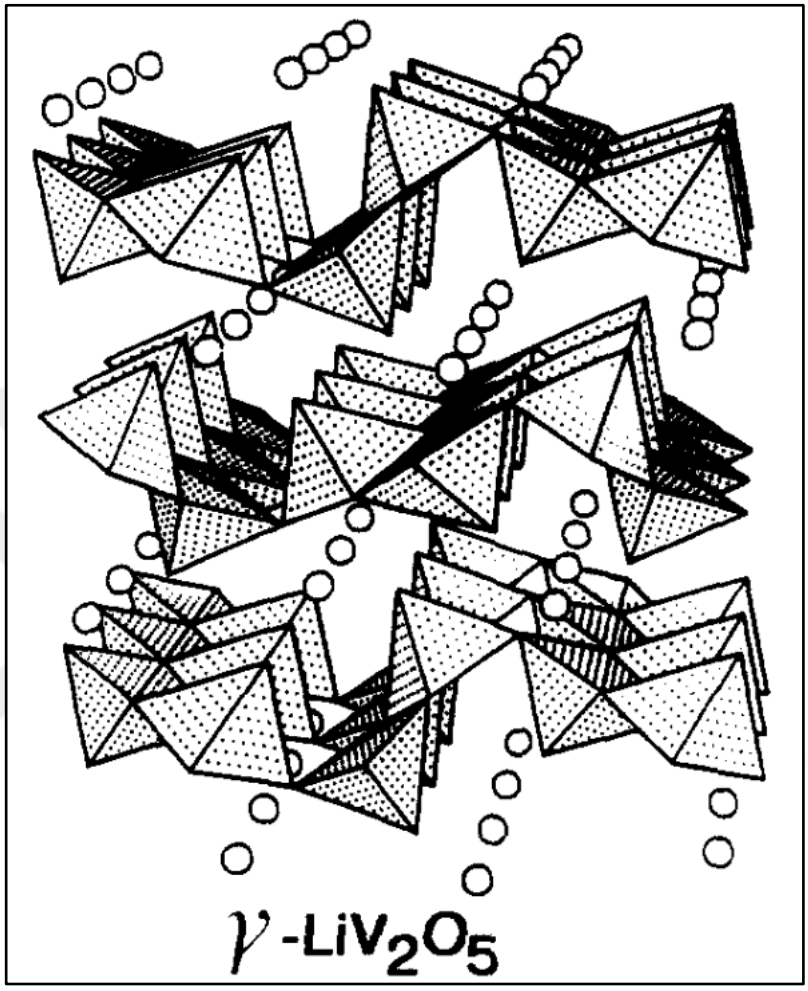

Figure 2.12: Schematic for structure of γ-V_2O_5.

Throughout the deep discharge of the Li//V_2O_5 cell, 3 li-ions can be intercalated into the structure. A new voltage plateau around 2.1 V is observed and ω-$Li_xV_2O_5$ phase transformation occurs. The outcome of this phase transformation is 440 mAh/g, which is a significant theoretical capacity value. ω-$Li_xV_2O_5$ suffers an irreversible loss of capacity after the first cycle because part of intercalated lithium ions cannot be de-intercalated [2].

Main drawbacks of the V_2O_5 cathode material are low capacity retention caused by deterioration from lithium diffusion and, ionic conductivity and electronic conductivity being low. In literature, reduction of sizes of particles within the material

to nano-scale has been thoroughly investigated. Yu et al. manufactured mesoporous V_2O_5 nanofibers by using a process consists of electrospinning, sol-gel process and subsequent air annealing. The produced nanofibers had a radius of 175 nm and a specific total area of surface value of 97 m^2/g.

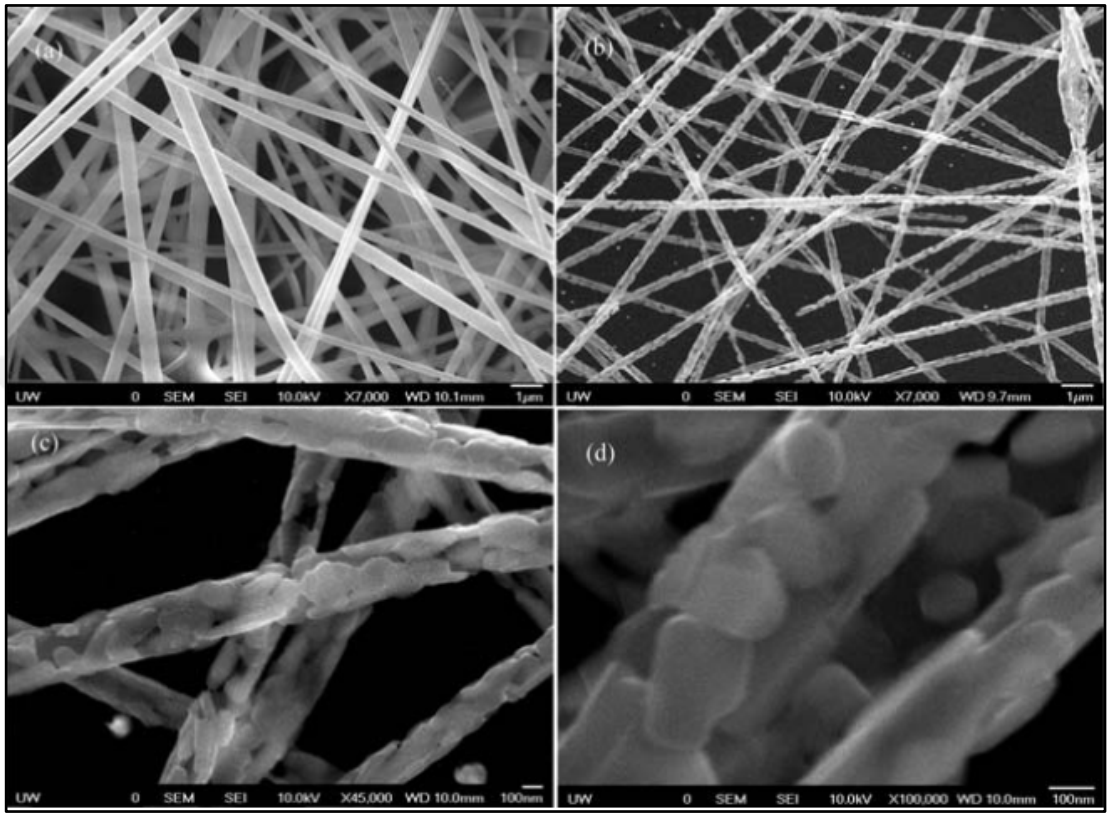

Figure 2.13: a) SEM images for V_2O_5 prior to annealing. b-d) Following a one-hour thermal treatment in air at 500 °C, SEM pictures of V_2O_5.

At high current densities they reported specific capacity of 370 mAh/g. Material suffered a capacity loss after 10^{th} cycle, between 10^{th} and 40^{th} cycle excellent capacity retention was reported [48].

Mai et al. investigated vanadium oxide nanowires produced using electrospinning and annealing. Resulting novel nanostructure, constructed by attached nanorods, had radiuses between 50 nm and 100 nm and lengthiness of up to extend of millimeters. They conducted cycling between 1.75 and 4 V for one set and 2 and 4 V for another set. For the first set, they reported 390 mAh/g initial discharge capacity and 201 mAh/g discharge capacity at 50^{th} cycle. For the second set, 275 mAh/g initial discharge capacity and 187 mAh/g discharge capacity at 50^{th} cycle was reported. By employing the suggested nanostructure, the self-aggregation of nanomaterials was

reduced, leading to increased cycle stability as well as capacity in comparison to nanorods [49].

In literature, nanobelts and nanosheets have also been investigated as promising nanostructures for V_2O_5 cathode materials [50], [51]. Wang et al. used $V_2O_5 \cdot H_2O$ nanoseeds and produced a V_2O_5 nanobelt array on a titanium substrate. They cycled the prepared cells at current density of 400, 1000 and 4000 mA/g. They reported 230, 180 and 150 mAh/g discharge capacity for 50 cycles at 400, 1000 and 4000 mA/g current density, respectively. Since the nanomaterial was constructed on a conductive surface, processes regarding preparing the electrodes could be bypassed [52].

Rui et al. used a liquid exfoliation to synthesize V_2O_5 nanosheets range in thickness from 2.1 to 3.8 nm. They reported 290 mAh/g initial discharge capacity at 2 C current density and 274 mAh/g discharge capacity at 50^{th} cycle. The proposed material had 93.8% capacity retention while intercalating 2 lithium ions. The electrochemical improvements to the material compared were credited to large specific surface are of the proposed nanostructure and short diffusion pathways [53].

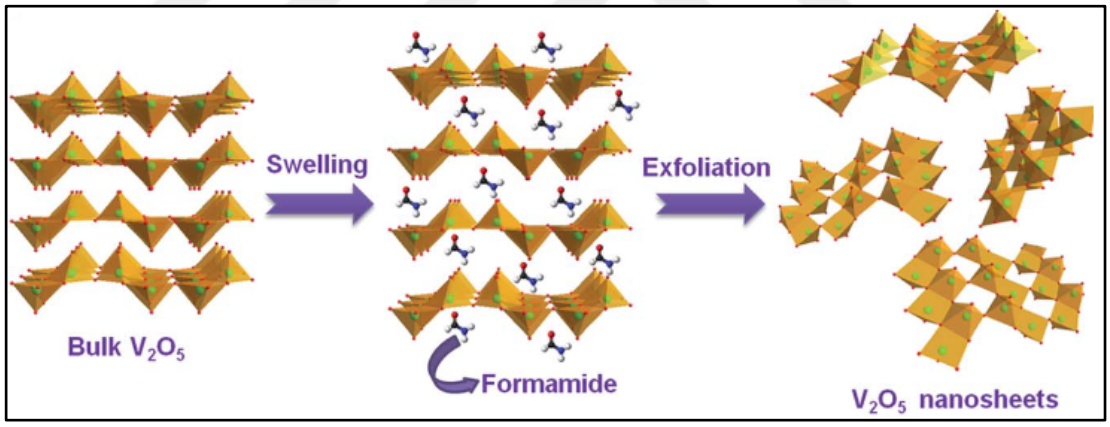

Figure 2.14: Schematic of nanosheet synthesis.

Other than employing nanostructures, doping V_2O_5 with cations is investigated to modify the valence state of vanadium in order to increase electrical conductivity and improve lithium-ion transport across the crystal lattice of V_2O_5. Li et al. used sol-gel process and subsequent annealing for two hours in the air at 450°C to produce tin doped V_2O_5 film. They reported 334 mAh/g specific capacity at 500 mA/g current density after 50 cycles, compared to 157 mAh/g specific capacity of pure V_2O_5 film. They concluded the enhancement of the electrochemical performance was due to increased conductivity caused by lower valence state of the vanadium ions,

stabilization of VO_5 caused by the presence of Sn^{4+} ions [54]. In literature, other than Sn doping of other ions such as Mn, Cu and Cr has also been investigated [55], [56] [57].

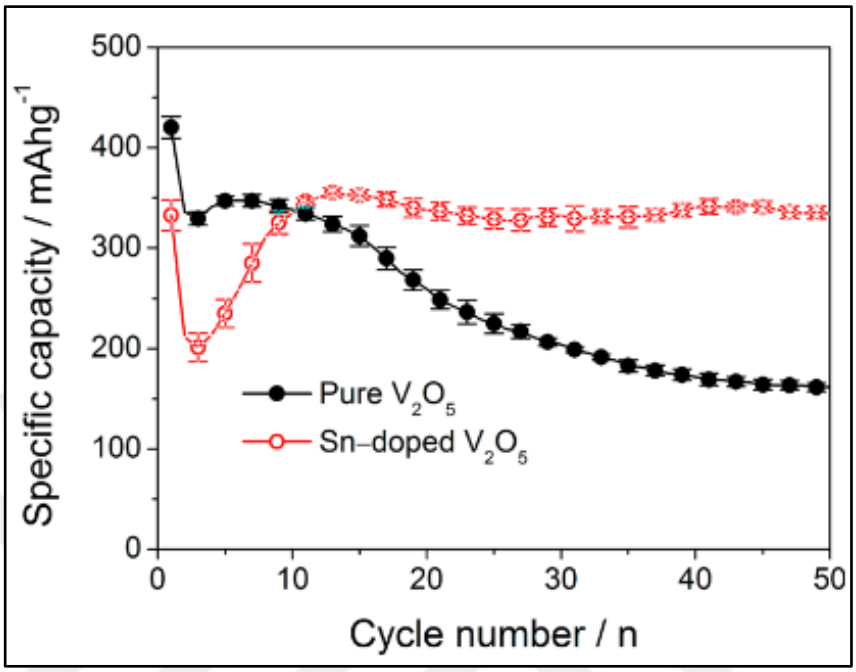

Figure 2.15: Performance of pure and Sn-doped V_2O_5 during cycling at 500 mA/g current density.

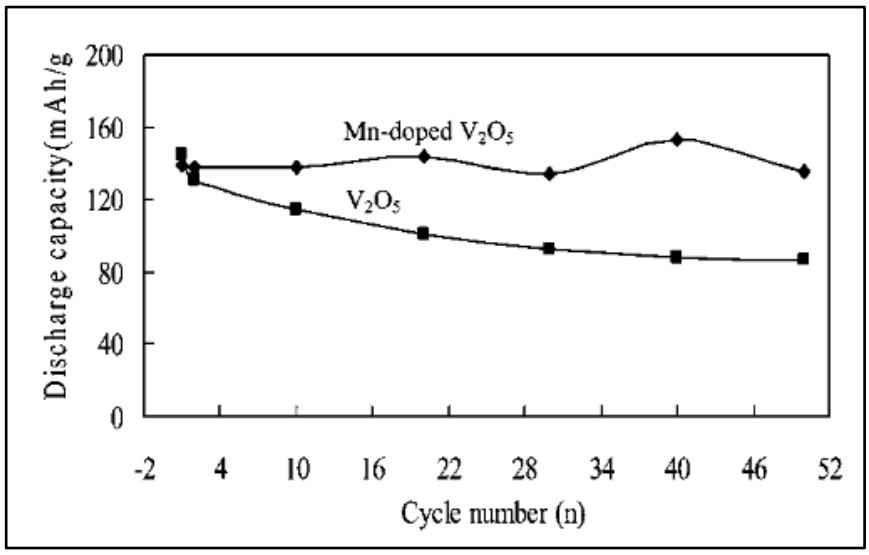

Figure 2.16: Performance of pure and Mn-doped V_2O_5 during cycling at 680 mA/g current density.

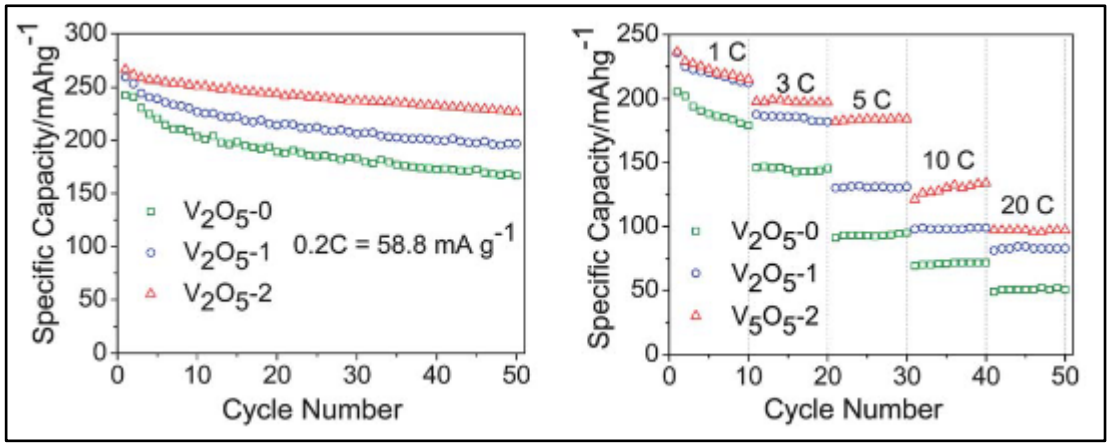

Figure 2.17: Cycling performance of proposed 3 materials at 58.8 mA/g current density and at varying current density values between 1 C and 20 C.

To improve the electrochemical characteristics of the material, Rui et al. researched the effects of reduced graphene oxide. They used a solvothermal method and an annealing procedure to synthesize extremely porous polycrystalline V_2O_5 spheres supported by reduced graphene oxide. The V_2O_5/rGO composites demonstrated outstanding rate capability, little capacity fading, and enhanced battery performance with high specific capacities. A satisfactory 85% capacity retention value at 50^{th} cycle, at about 0.3C and a potential range between 2 and 4 V was attained by the V_2O_5 and 46% by weight rGO composite. Regarding high rate functionality, these samples was cycled using 13 C and 19 C current rates and specific capacities of 128 and 102 mAh/g were achieved, respectively. The innovative V_2O_5/rGO composite structures, with their high electric conductivity, rapid lithium diffusion, simple electrolyte penetration, and strong structural stability, led to the remarkable battery performance.

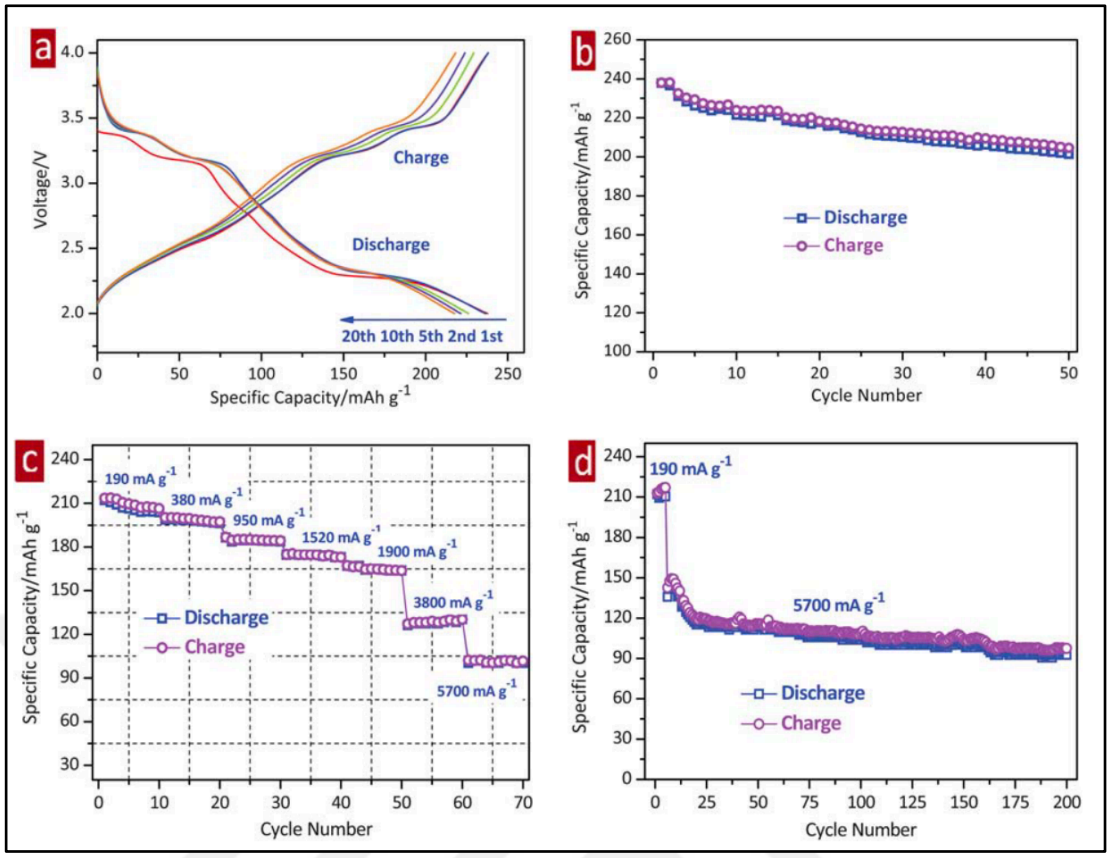

Figure 2.18: a) Galvanostatic charge-discharge curves of the V_2O_5/rGO (46 wt%) cathode material at 90 mA/g current density. b) Cycling performance of the material at 90 mA/g current density c) Cycling performance of the material at varying current densities between 190 to 5700 mA/g. d) Cycling performance of the material at 5700 mA/g current density.

Afyon et al. proposed a novel approach to improve the electrochemical characteristics of V_2O_5 cathode material. They investigated V_2O_5–$LiBO_2$ glass and rGO/V_2O_5–$LiBO_2$ glass composite electrodes. They synthesized the glass material by using a glass forming process The active material is ball-milled with graphite oxide and then reduced with heat. V_2O_5–$LiBO_2$ glass material was cycled at 50,100 and 200 mA/g current density for and around 293, 236 and 180 mAh/g specific capacity was achieved, respectively. To improve the reaction kinetics of the material, they employed rGO/ V_2O_5–$LiBO_2$ glass composite electrodes. After cycling the composite electrode, they reported 405 mAh/g initial discharge capacity and approximately 300 mAh/g discharge capacity at 100th cycle using 50 mA/g current density [2].

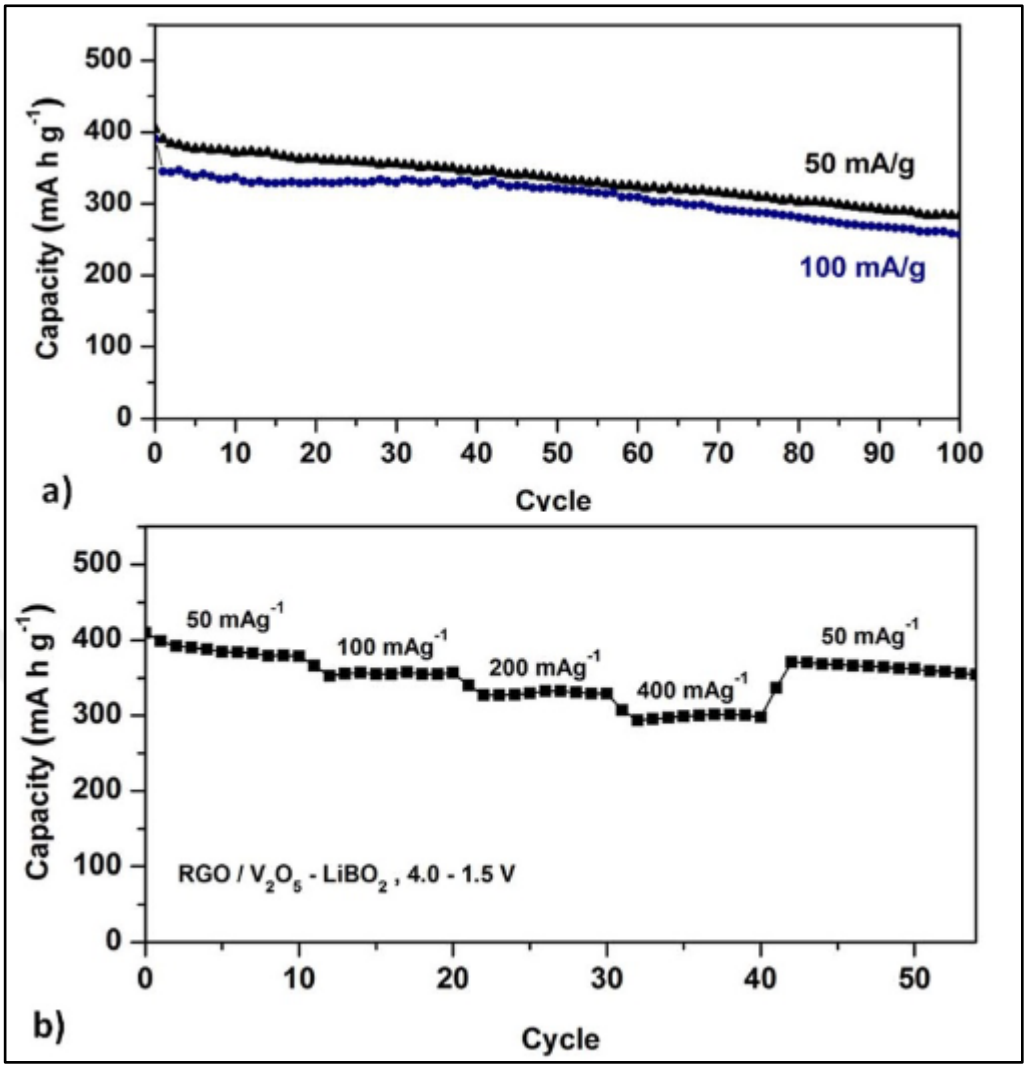

Figure 2.19: a) Cycling performance of rGO/V_2O_5–$LiBO_2$ glass composite at 50 and 100 mA/g current densities. b) Rate capability of the proposed material using 50, 100, 200 and 400 mA/g current density values.

3. EXPERIMENTAL

In this thesis a novel cathode material for LIBs based on V_2O_5 is investigated. V_2O_5 has been chosen as the investigated material as a result of numerous valence states of vanadium which results in high theoretical specific capacity compared to commercial cathode materials like $LiCoO_2$ and $LiFePO_4$. To solve the main drawbacks of the material, low capacity retention caused by irreversible structural transformations and low ionic-electronic conductivity, glassy V_2O_5 with rGO is proposed. In literature, the amorphous structure has been shown to improve the electrochemical performance of the V_2O_5 [2]. Employing composite electrodes with rGO has been shown to enhance the electrochemical characteristics of the V_2O_5 because of the extremely conductive essence of the rGO [3]. Based on the literature review conducted in the scope of this thesis, a V_2O_5-B_2O_3 glassy material with rGO is proposed as the LIB cathode material. Under the topic of experimental research, specific details regarding the materials employed in the tests, the circumstances under which they were conducted, their methodology, and applied characterizations will be provided. Figure 3.1. illustrates the workflow of the study.

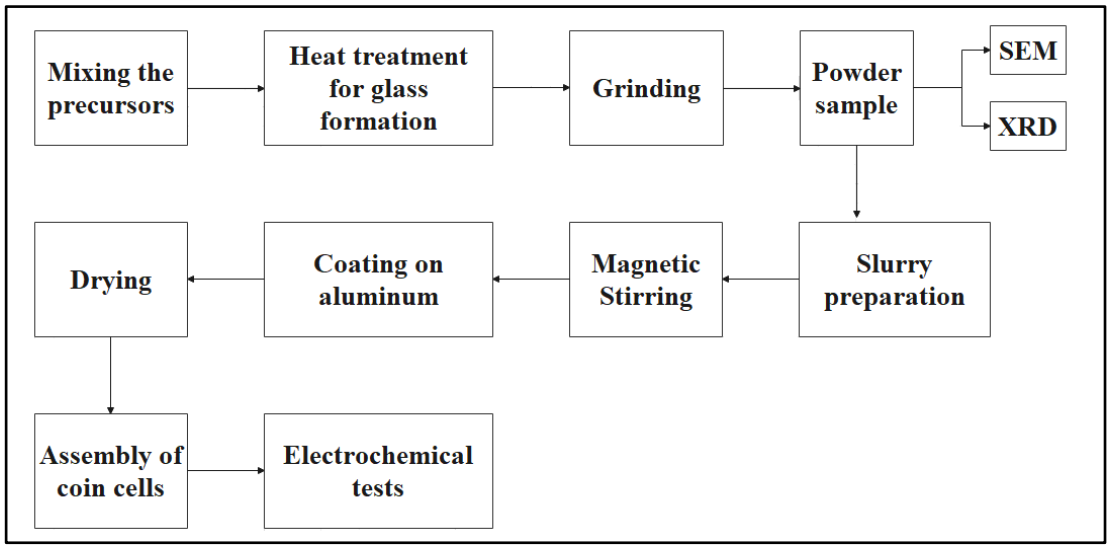

Figure 3.1: Flowchart of the study.

3.1. Chemicals Used in Experimental Work

Chemicals used in experimental work, their brand and their purities of the chemicals can be seen in Table 3.1.

Table 3.1: Chemicals used in experimental work.

Chemical	Brand
V_2O_5	Alfa Aesar
B_2O_3	Alfa Aesar
EC	Alfa Aesar
DMC	Sigma Aldrich
$LiPF_6$	Sigma Aldrich
Carbon black	MTI
PVDF	MTI
RGO	Hazerfen
NMP	Merck

3.2. Equipment Used in Experimental Work

Equipment used in experimental work, their brand and model can be seen in Table 3.2.

Table 3.2: Equipment used in experimental work.

Equipment	Brand
Furnace	MTI
Magnetic stirrer	Heidolph
Analytical balance	Acculab
Glovebox	Vigor
Press	MTI
Battery testing	Neware

3.3. Synthesis of Active Material

V_2O_5-B_2O_3 glass was synthesized using glass forming process [58]. Firstly, Alfa Aesar V_2O_5 (%99) and Alfa Aesar B_2O_3 (%99) analytical pure grade precursors for three compositions (80:20 wt-% V_2O_5:B_2O_3, 85:15 wt-% V_2O_5:B_2O_3, 90:10 wt-% V_2O_5:B_2O_3,) were mixed and pulverized using mortar and pestle. The ground powder was placed in alumina crucibles for heat treatment. The heat treatment was done in two steps. The first was raising the temperature of the furnace to 850°C, which was done in 1 hour. The second step was heat treatment of the prepared powder at 850°C, for 2 hours. Following the secondary step of the heat treatment, obtained homogenous melts were quenched using copper plates for fast cooling of the material, which results in formation of the glass. After quenching, produced V_2O_5-B_2O_3 glass was pulverized using mortar and pestle, to obtained powder for characterization and slurry preparation. The quantity of materials used for each composition can be seen in Table 3.3.

Table 3.3: Synthesized compositions and mass of the precursors used in synthesis.

Composition	Mass used for synthesis
80:20 wt-% V_2O_5:B_2O_3	8:2 g V_2O_5:B_2O_3
85:15 wt-% V_2O_5:B_2O_3	8.5:1.5 g V_2O_5:B_2O_3
90:10 wt-% V_2O_5:B_2O_3	9:1 g V_2O_5:B_2O_3

Figure 3.2: Quenched V_2O_5-B_2O_3 glass.

3.4. Preparation of Slurry

Preparation of slurry was completely carried out inside the Ar filled glovebox, because of air sensitivity of the V_2O_5-B_2O_3 glass. During the experiments, first batch of synthesized material has shown poor electrochemical performance, which was later fixed by conducting the rest of the process in inert atmosphere. Active materials, binders, and conductive agents were used to create cathodes, for ensuring high mechanical stability and electrical conductivity. N-methyl-2-pyrrolidone (NMP) was used to dissolve the binder, polyvinylidene fluoride (PVDF). The conductive agents were carbon black and reduced graphite oxide (rGO) . V_2O_5-B_2O_3 glass, carbon black, rGO, and polyvinylidene fluoride (PVDF) were combined at the proper mass ratios to create the electrode slurry. Ground V_2O_5-B_2O_3 glass, carbon black, PVDF and rGO were mixed and ground using agate mortar with weight ratios of 70%, 5%, 10%, 15%, respectively. The resulting powder was mixed with NMP, then stirred overnight (approximately 24 hours) using a magnetic stirrer. The slurry was coated on aluminum, and dried for approximately 48 hours.

Table 3.4: Materials and their mass used in preparation of slurry.

Precursor	Mass
V_2O_5-B_2O_3 glass	140 mg
rGO	30 mg
PVDF	20 mg
Carbon black	10 mg

Figure 3.3: Aluminum coated with slurry.

3.5. Assembly of Coin Cells

For conducting the electrochemical tests, coin cells were assembled using the prepared cathode working against lithium metal as anode. Firstly, the dried slurry on aluminum was cut in the shapes of circles with diameter of 1.1 cm to obtain electrode disks. The electrode disks are weighted, and the weight of active material for each sample is noted. Approximately 5 mg/cm^2 loading was achieved for each sample. 1 M

$LiPF_6$ in solution of 1:1 EC-DMC was used as electrolyte. The assembly process was carried out in Ar filled glovebox with impurity levels below 1 ppm for O_2 and H_2O. Figure 3.4. depicts a diagram of the coin cell assembly [59].

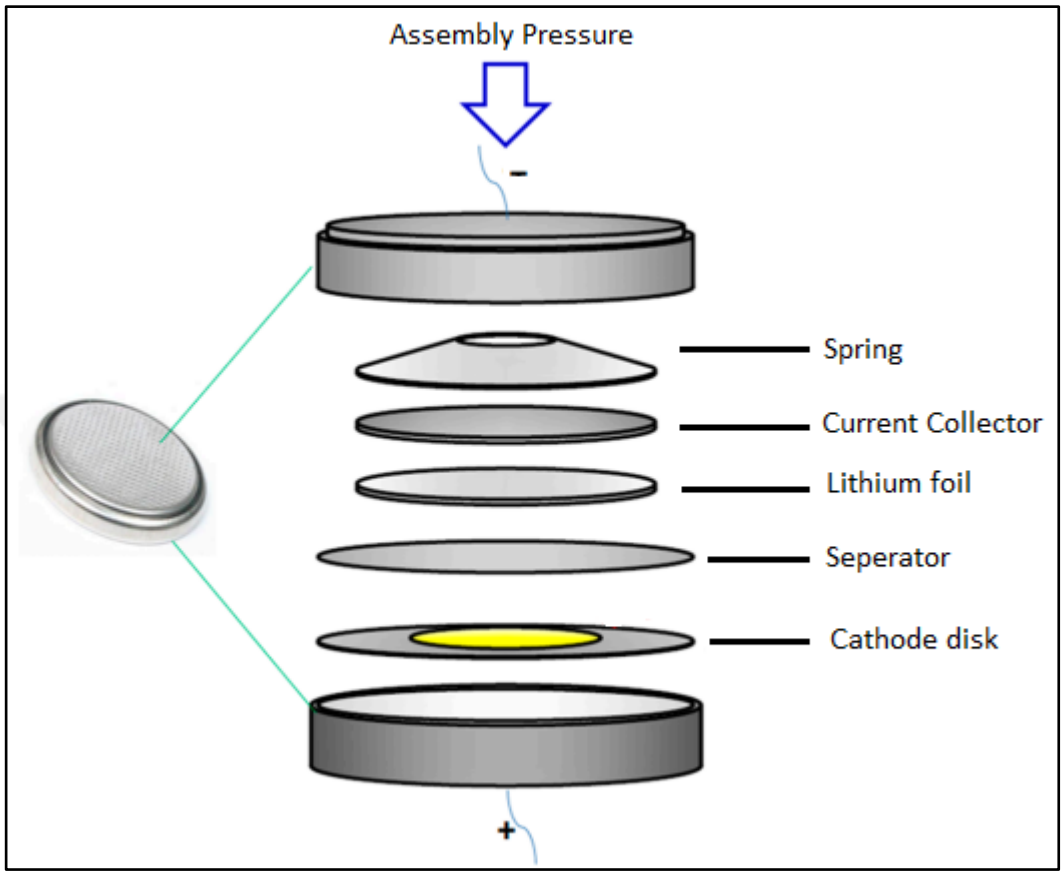

Figure 3.4: Schematic representation for assembly of a coin cell.

4. RESULTS AND DISCUSSION

In this section, results of experimental work and characterization of the synthesized materials are reviewed. For each material, charge-discharge curves for the first 10 cycles, the rate capability at constant current density, and rate capability at varying current densities are investigated. The electrochemical tests are conducted within the potential window of 1.5-4 V. Since no lithium is present in the V_2O_5-B_2O_3 glass, before each test cells are discharged against lithium for lithiation of the materials. In the course of computation of specific capacity values total mass of V_2O_5-B_2O_3 was glass considered.

4.1. 80:20 wt-% V_2O_5:B_2O_3 Glass

4.1.1. Electrochemical Tests

The first galvanostatic cycling test is conducted within the potential range of 1.5-4 V at 50 mA/g current density. For the first 10 charge-discharge cycles, the material had specific capacity values around 200 mAh/g, peaking at 207 mAh/g and dipping at 190 mAh/g. This specific capacity values suggests more than one lithium ion was intercalated and de-intercalated, since theoretical capacity of the V_2O_5 is 294 mAh/g for 2 lithium ions and 147 mAh/g for 1 lithium ions.

The cell is cycled for 100 cycles at 50 mA/g constant current density. For the first 20 cycles, no significant dip in specific capacity was seen, which suggests an improvement over bulk V_2O_5 cathode material since the bulk material suffers a significant capacity loss after 10 cycles. After 100 cycles, the cell had around 120 mAh/g specific capacity which translates to roughly 60% capacity retention.

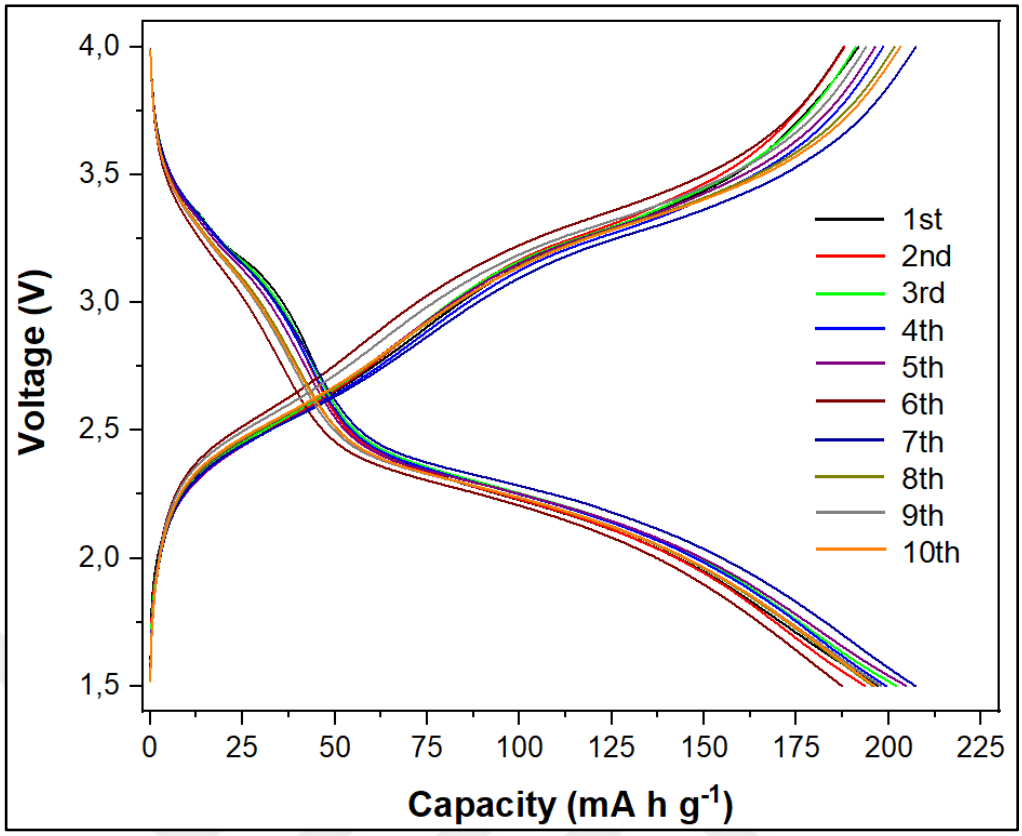

Figure 4.1: Charge-discharge curves of 80:20 wt-% V_2O_5:B_2O_3 glass for first 10 cycles within the potential range of 1.5-4 V at 50 mA/g current density.

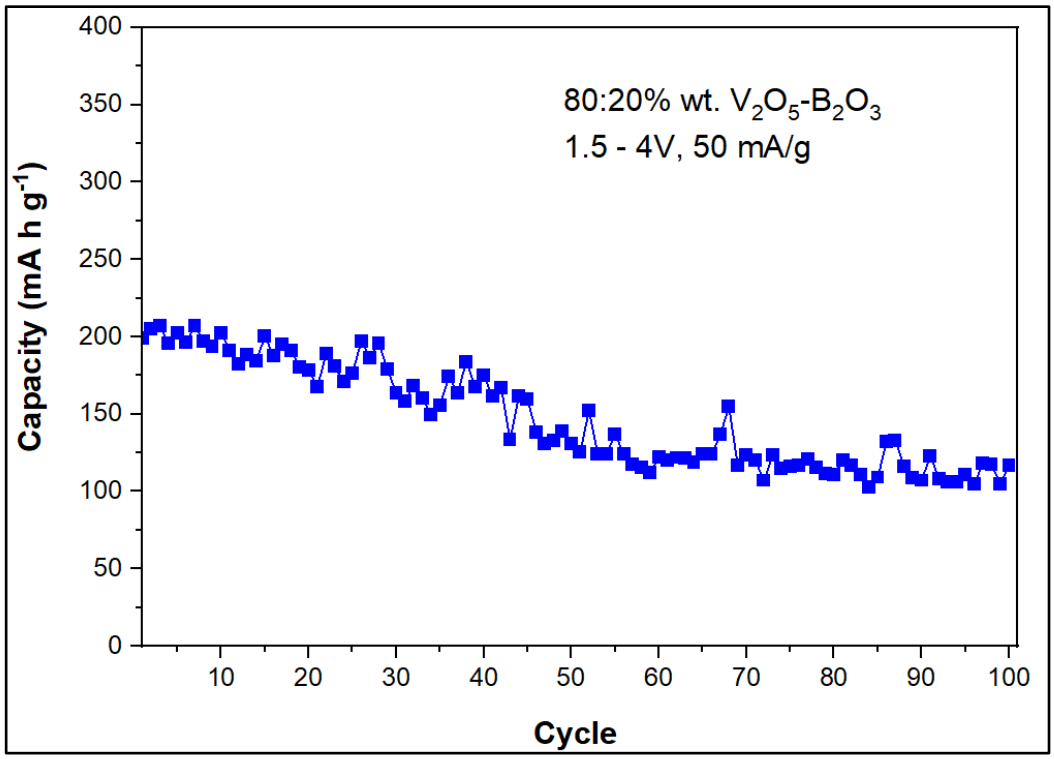

Figure 4.2: Cycling performance of the 80:20 wt-% V_2O_5:B_2O_3 glass after 100 cycles within the potential range of 1.5-4 V at 50 mA/g current density.

To investigate rate capability, cell is cycled with varying current densities. 50, 100, 200 and 50 mA/g current density was used for 10 cycling blocks. With 100 mA/g current density 100 mAh/g specific capacity was achieved. The material had around 50 mAh/g specific capacity for 200 mA/g current density. When the cell was cycled with 50 mA/g current density at the last cycling block, specific capacity between 125 and 150 mAh/g was achieved. This galvanostatic cycling test proves an improved cycling ability over bulk V_2O_5 cathode material.

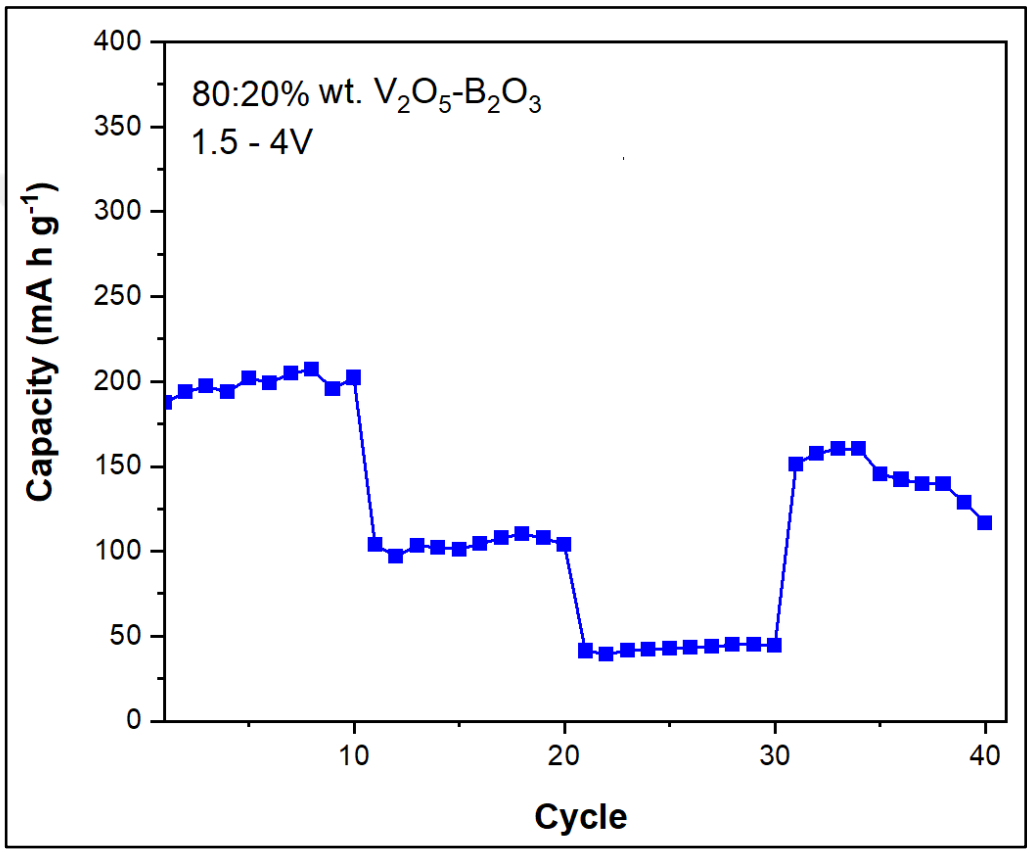

Figure 4.3: Cycling performance of the 80:20 wt-% V_2O_5:B_2O_3 glass material for varying current densities within the potential range of 1.5-4 V.

4.1.2. X-Ray Diffraction Patterns

In Figure 4.4. XRD patterns of 80:20 wt-% V_2O_5:B_2O_3 can be seen. The diffraction peaks of V_2O_5 appeared at $2\theta = 20.24°$, 26.88° and 31.14°. No diffraction peaks for B_2O_3 can be seen, which suggests the structure is not purely glass, but crystalline and glassy. These results show that the 80:20 wt-% V_2O_5:B_2O_3 is note purely glass, but a glassy material.

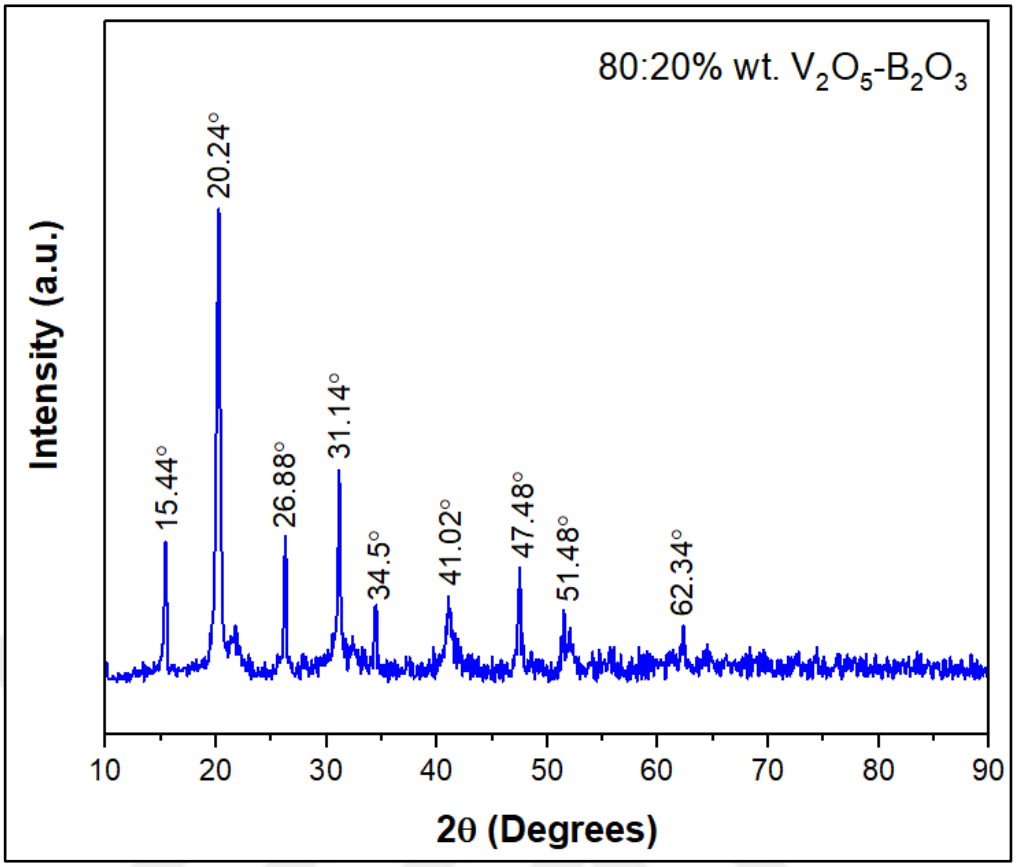

Figure 4.4: XRD patterns of 80:20 wt-% V_2O_5:B_2O_3.

4.1.3. Scanning Electron Microscope Images

The SEM images for 80:20 wt-% V_2O_5:B_2O_3 sample shows inhomogenities in particle size. Crystallinity can also be seen in SEM images, which shows that material is not in pure glass structure, but a glassy material.

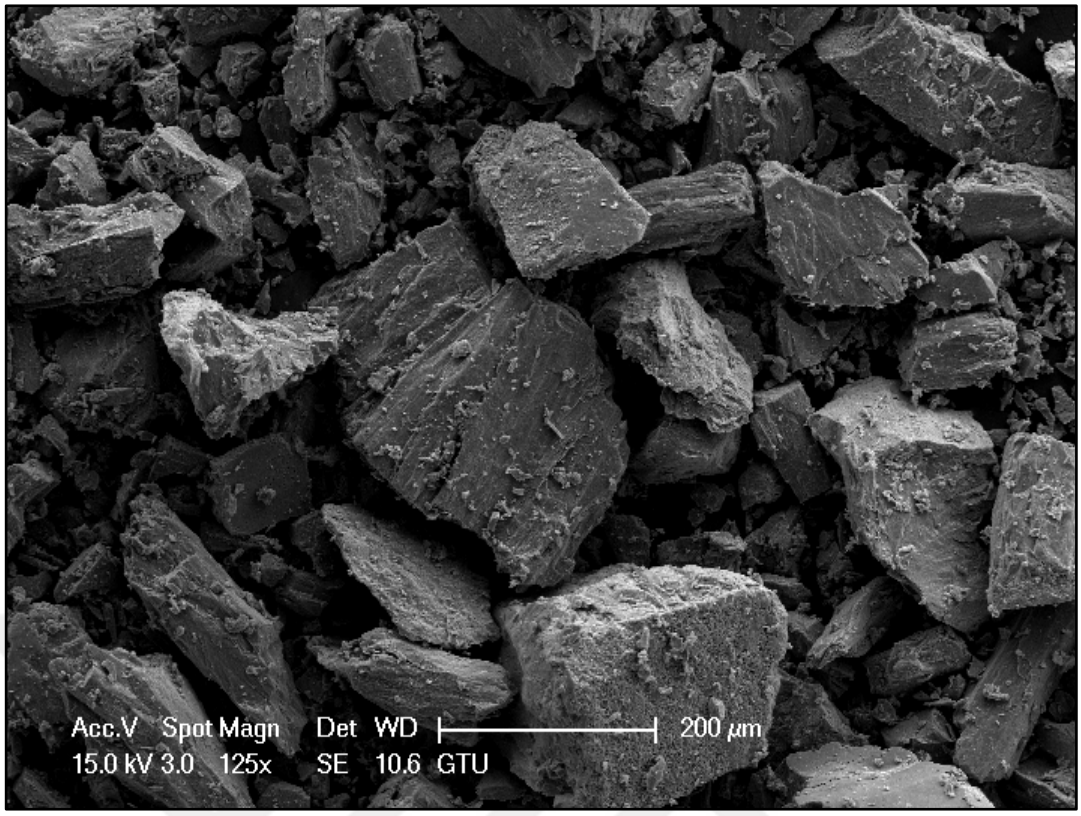

Figure 4.5: SEM images of 80:20 wt-% V_2O_5:B_2O_3.

4.2. 85:15 wt-% V_2O_5:B_2O_3 Glass

4.2.1. Electrochemical Tests

For the first 10 charge-discharge cycles, the material had specific capacity values around 210 mAh/g, peaking at 222 mAh/g and dipping at 205 mAh/g. This specific capacity values suggests more than one lithium ion was intercalated and de-intercalated. First 10 cycles of the material show 85:15 wt-% V_2O_5:B_2O_3 has higher specific capacity than 80:20 wt-% V_2O_5:B_2O_3.

The cell is cycled for 100 cycles at 50 mA/g constant current density. The cell had 205 mAh/g specific capacity at 27^{th}, after that cycle capacity loss occurs. After 100 cycles, the cell had around 135 mAh/g specific capacity which translates to roughly 64% capacity retention.

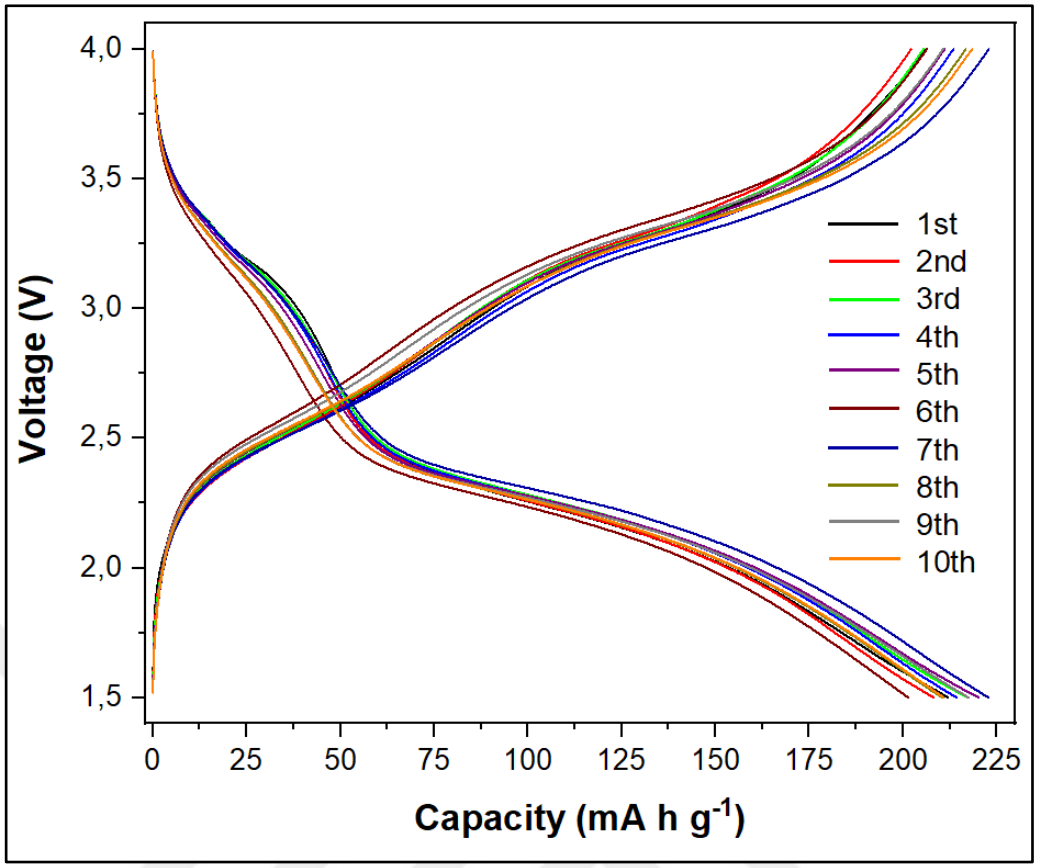

Figure 4.6: Charge-discharge curves of 85:15 wt-% V_2O_5:B_2O_3 glass for first 10 cycles within the potential range of 1.5-4 V at 50 mA/g current density.

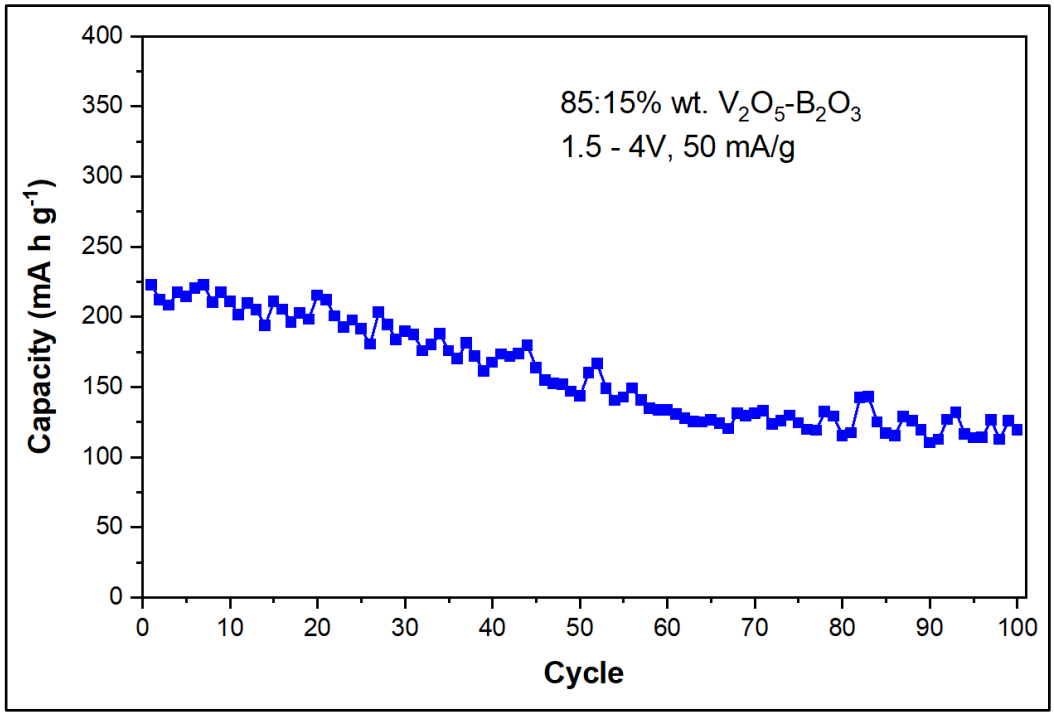

Figure 4.7: Cycling performance of the 85:15 wt-% V_2O_5:B_2O_3 glass after 100 cycles within the potential range of 1.5-4 V at 50 mA/g current density.

To investigate the rate capability, cell is cycled with varying current densities. 50, 100, 200 and 50 mA/g current density was used for 10 cycling blocks. With 100 mA/g current density 115 mAh/g specific capacity was achieved. The material had around 50 mAh/g specific capacity for 200 mA/g current density. When the cell was cycled with 50 mA/g current density at the last cycling block, specific capacity between 135 and 172 mAh/g was achieved.

Results of cycling at constant current density and varying current densities suggests 85:15 wt-% V_2O_5:B_2O_3 has better cycling performance than 80:20 wt-% V_2O_5:B_2O_3.

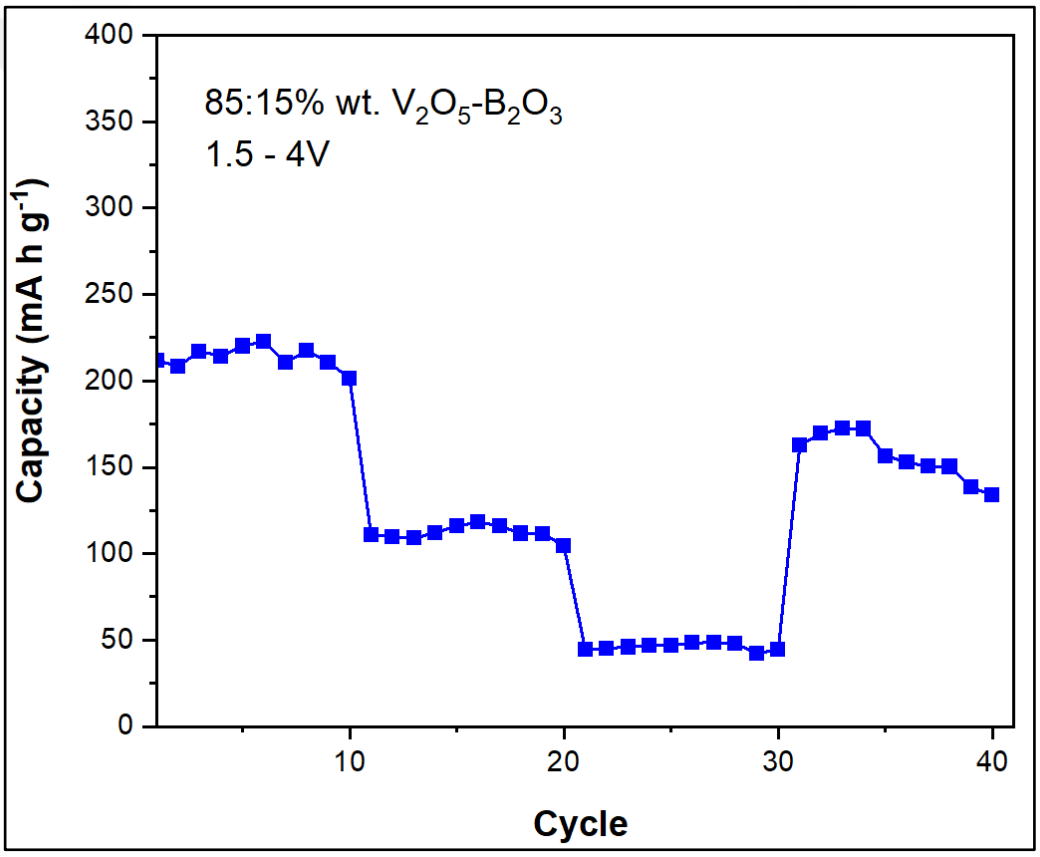

Figure 4.8: Cycling performance of the 85:15 wt-% V_2O_5:B_2O_3 glass material for varying current densities within the potential range of 1.5-4 V.

4.2.2. X-Ray Diffraction Patterns

In Figure 4.8. XRD patterns of 85:15 wt-% V_2O_5:B_2O_3 can be seen. The diffraction peaks of V_2O_5 appeared at $2\theta = 20.18°$, 26.18° and 31.06°. No diffraction

peaks for B_2O_3 can be seen, which suggests the structure is not purely glass, but crystalline and glassy. These results show that the 80:20 wt-% V_2O_5:B_2O_3 is note purely glass, but a glassy material.

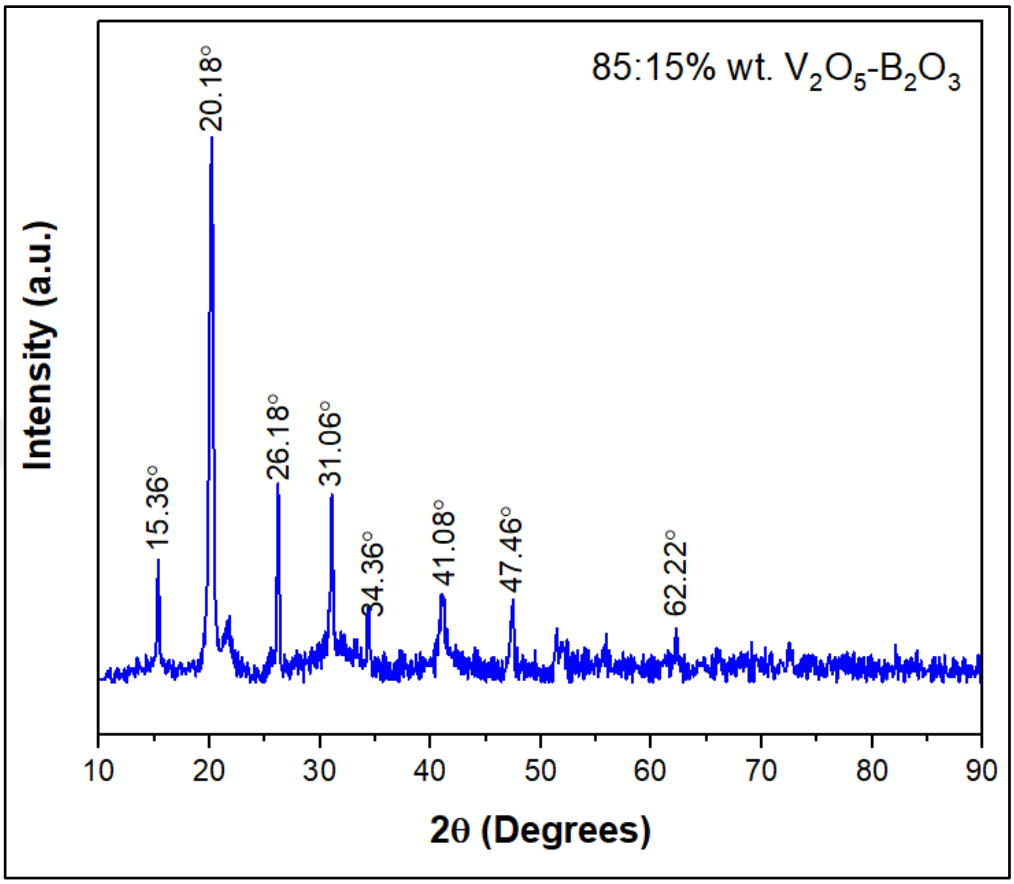

Figure 4.9: XRD patterns of 85:15 wt-% V_2O_5:B_2O_3.

4.2.3. Scanning Electron Microscope Images

The SEM images for 85:15 wt-% V_2O_5:B_2O_3 sample shows inhomogenities in particle size, but particle sizes are closer to each other compared to 80:10 and 90:10 wt-% V_2O_5:B_2O_3. Crystallinity can also be seen in SEM images, which shows that material is not in pure glass structure, but a glassy material.

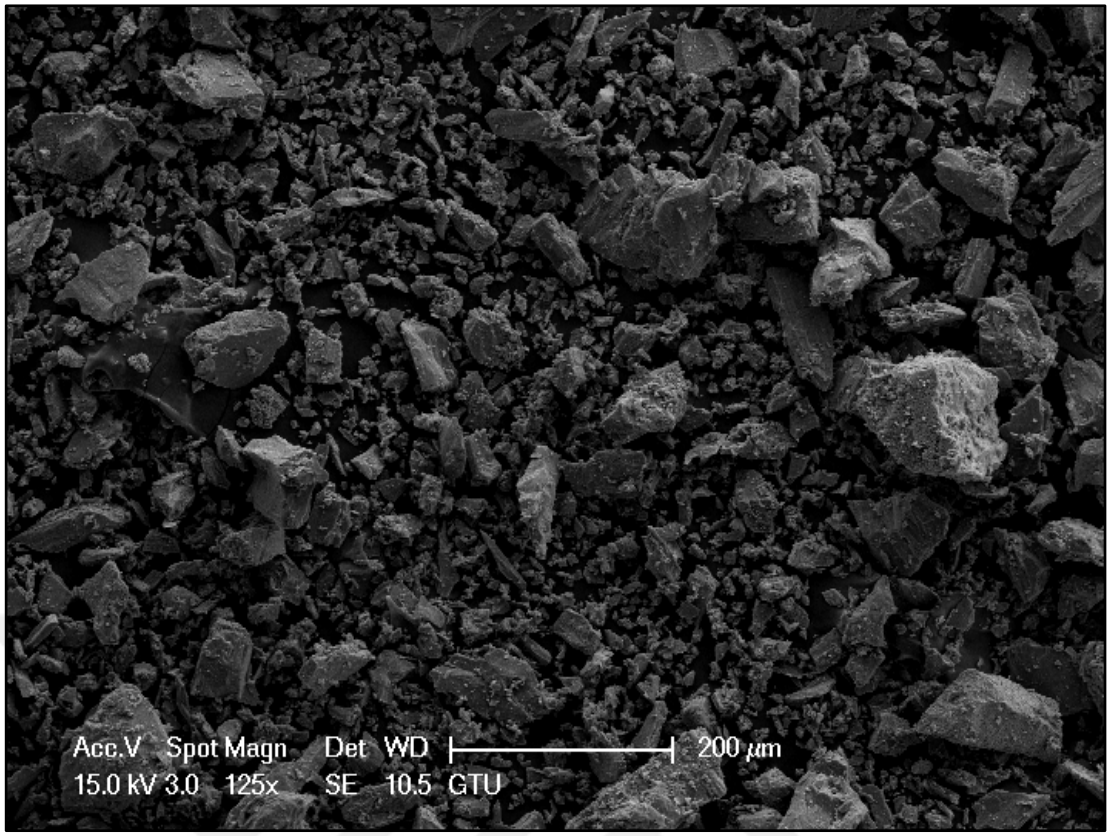

Figure 4.10: SEM images of 85:15 wt-% V_2O_5:B_2O_3.

4.3. 90:10 wt-% V_2O_5:B_2O_3 Glass

4.3.1. Electrochemical Tests

For the first 10 charge-discharge cycles, the material had specific capacity values around 180 mAh/g, peaking at 191 mAh/g and dipping at 171 mAh/g. This specific capacity values suggests more than one lithium ion was intercalated and de-intercalated. First 10 cycles of the material show 90:10 wt-% V_2O_5:B_2O_3 has the lowest specific capacity among all of the investigated materials.

The cell is cycled for 100 cycles at 50 mA/g constant current density. The cell had 182 mAh/g specific capacity at 20^{th}, after that cycle capacity loss occurs. After 100 cycles, the cell had around 103 mAh/g specific capacity which translates to roughly 53% capacity retention.

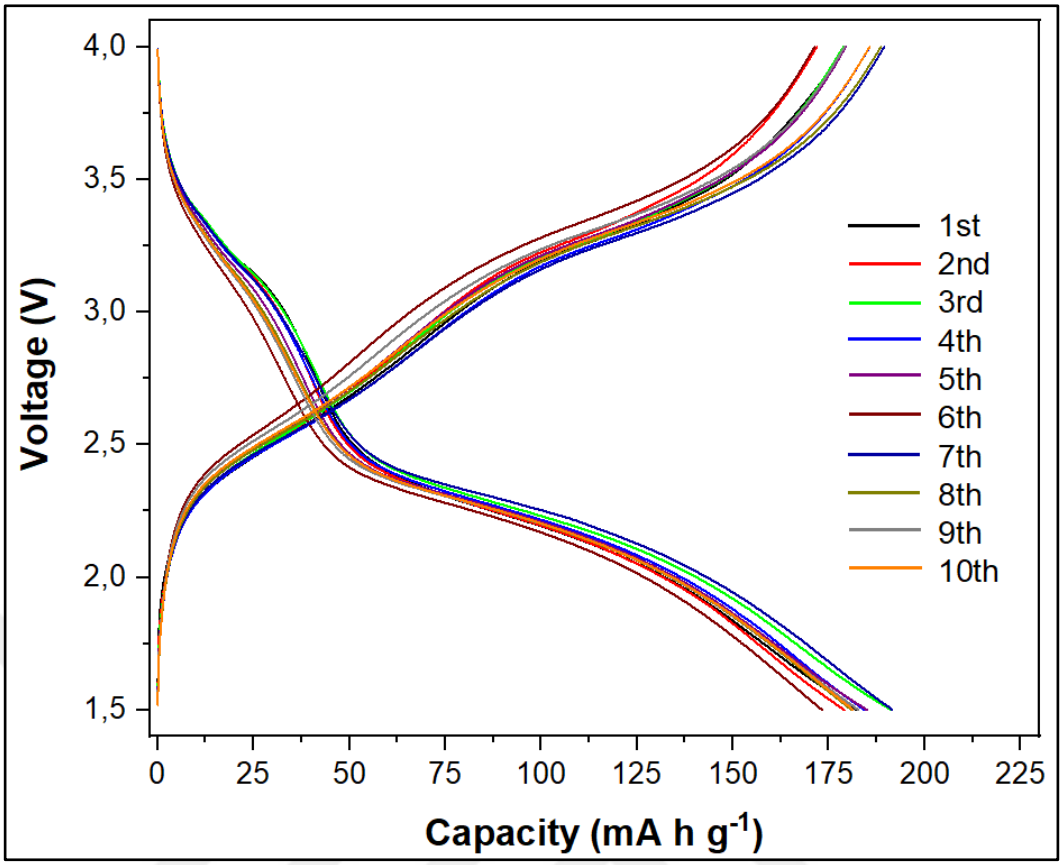

Figure 4.11: Charge-discharge curves of 90:10 wt-% V_2O_5:B_2O_3 glass for first 10 cycles within the potential range of 1.5-4 V at 50 mA/g current density.

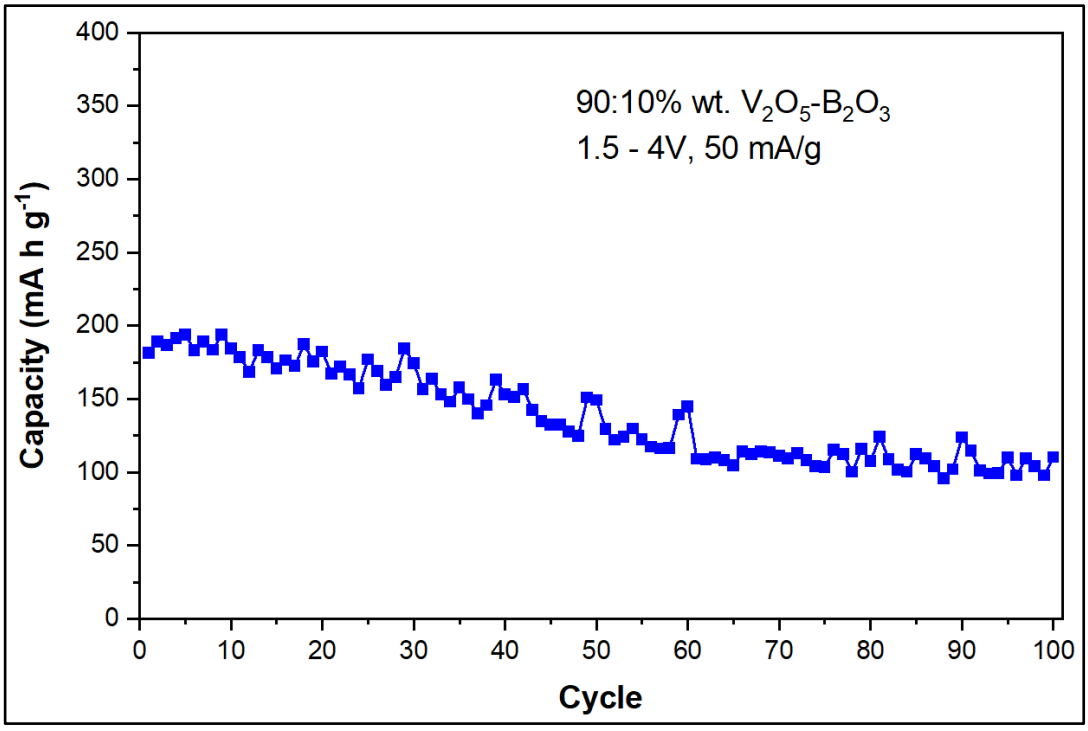

Figure 4.12: Cycling performance of the 90:10 wt-% V_2O_5:B_2O_3 glass after 100 cycles within the potential range of 1.5-4 V at 50 mA/g current density.

To investigate the rate capability, cell is cycled with varying current densities. 50, 100, 200 and 50 mA/g current density was used for 10 cycling blocks. With 100 mA/g current density between 92 and 102 mAh/g was achieved. The material had around 45 mAh/g specific capacity for 200 mA/g current density. When the cell was cycled with 50 mA/g current density at the last cycling block, specific capacity values between 133 and 171 mAh/g were achieved.

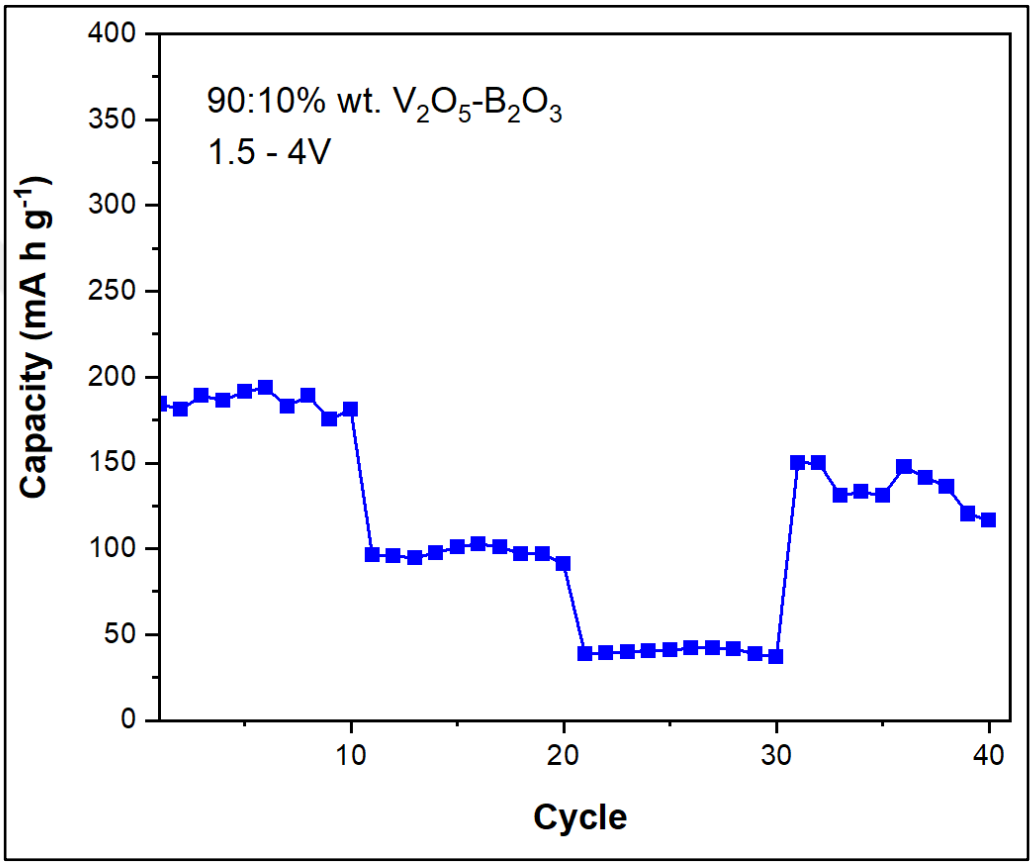

Figure 4.13: Cycling performance of the 90:10 wt-% V_2O_5:B_2O_3 glass material for varying current densities within the potential range of 1.5-4 V.

4.3.2. X-Ray Diffraction Patterns

In Figure 4.8. XRD patterns of 90:10 wt-% V_2O_5:B_2O_3 can be seen. The diffraction peaks of V_2O_5 appeared at 2θ = 15.51°, 20.37°, 26.35° and 31.18°. No diffraction peaks for B_2O_3 can be seen, which suggests the structure is not purely glass, but crystalline and glassy. These results show that the 80:20 wt-% V_2O_5:B_2O_3 is note purely glass, but a glassy material.

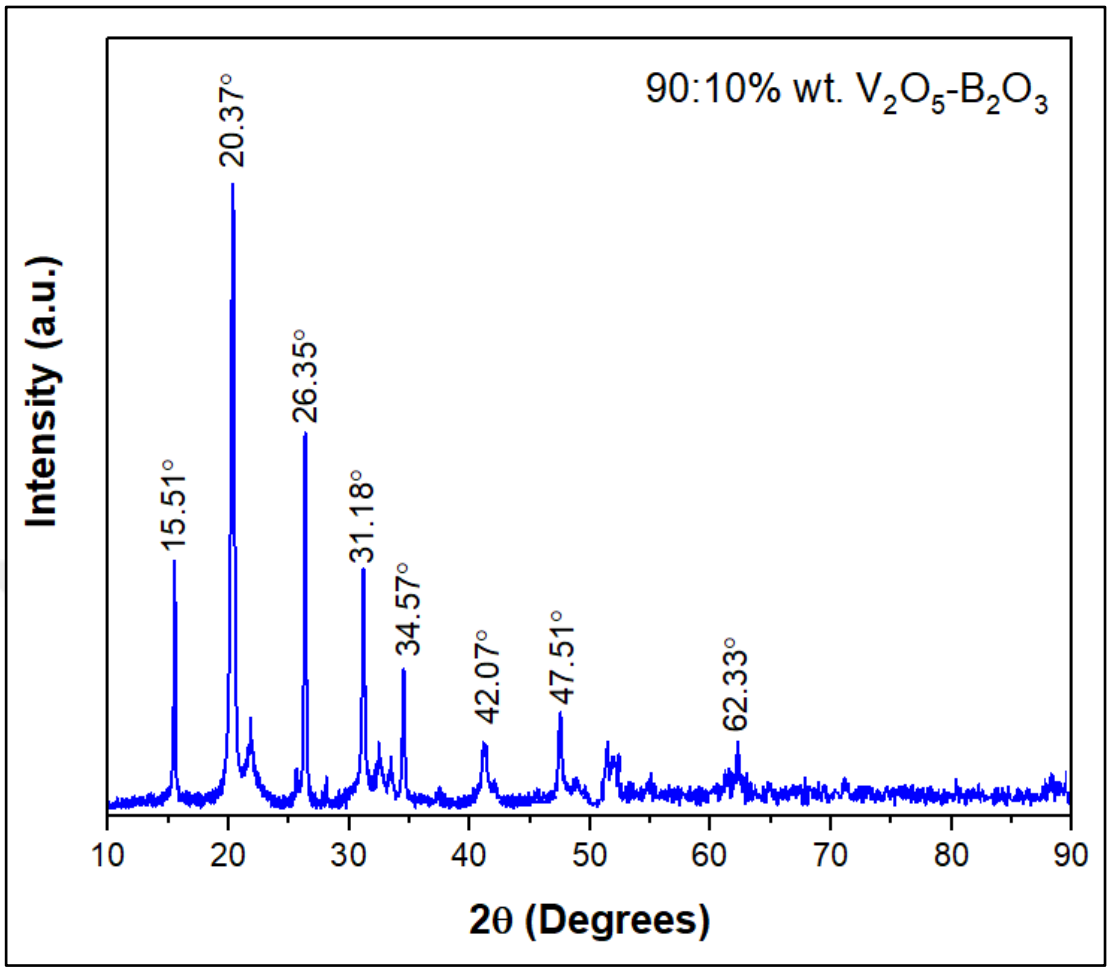

Figure 4.14: XRD patterns of 90:10 wt-% V_2O_5:B_2O_3.

4.3.3. Scanning Electron Microscope Images

The SEM images for 90:10 wt-% V_2O_5:B_2O_3 sample shows inhomogenities in particle size. Crystallinity can also be seen in SEM images, which shows that material is not in pure glass structure, but a glassy material.

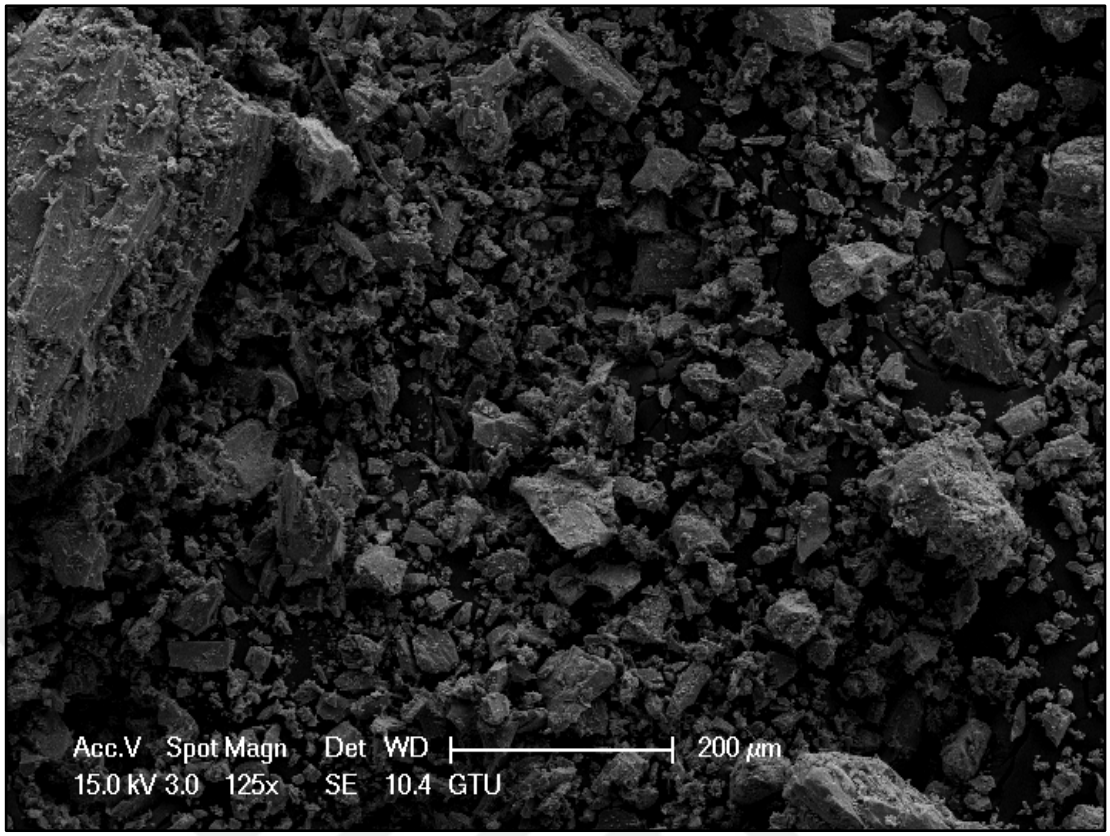

Figure 4.15: SEM images of 90:10 wt-% V_2O_5:B_2O_3.

5. CONCLUSION

In this thesis, V_2O_5-B_2O_3 glassy material was synthesized with V_2O_5 and B_2O_3 precursors using glass forming process. In this glass system, the vanadate glass network, which is made up of vanadium-oxygen tetrahedra, forms because the V2O5 level relatively is high compared to the B_2O_3 content. This structure improves the electrochemical performance of the V_2O_5 because the amorphous nature of the material prevents occurrence of irreversible phase transformations, which is one of the main drawbacks of the V_2O_5 when employed as a cathode material for LIBs. Three specimens with different weight ratios (80:20, 85:15, 90:10 wt-% V_2O_5:B_2O_3) were synthesized, electrochemical tests and characterization of the specimens were carried out. Since low ionic and electronic conductivity is another drawback of the V_2O_5, during the preparation of the cathode slurry in addition to carbon black, rGO was added as a conductive agent to further improve the conductivity of the electrode.

Galvanostatic cycling analysis for 3 materials were carried out. For all three of the materials, first 10 charge-discharge cycles were investigated. The cycling was done within the potential range of 1-4.5 V using 50 mA/g current density. 85:15 wt-% V_2O_5:B_2O_3 glass had the highest specific capacity, 222 mAh/g, followed by 80:20 at 207 mAh/g and 90:10 at 191 mAh/g. Since theoretical capacity of the V_2O_5 for 1 lithium-ion intercalation/de-intercalation was calculated as 147 mAh/g, these specific capacity values suggest that more than 1 lithium-ion per formula was intercalated and de-intercalated. The predicted homogeneous phase lithiation process of a glass material is compatible with the appearance of featureless curves without a multi-step behavior. The resulting specific capacity values are higher than the specific capacity value of commercial cathode materials such as $LiCoO_2$ and $LiFePO_4$.

Bulk V_2O_5 when used as a cathode for LIBs suffers a significant capacity loss after 10 cycles. The proposed V_2O_5:B_2O_3 glass had almost no capacity loss after 10 cycles, furthermore when cycled for 100 cycles, materials had reasonable capacity retention. The cells were cycled with varying current densities to investigate the rate capability of the material. 10 cycling blocks with 50, 100, 200 and 50 mA/g current densities were used for this test. Specific capacity of the material suffers a severe drop at 200 mA/g current density but recovers when 50 mA/g current density is used again.

Poor kinetics of the glassy material is likely to be the source of limited capacities at high current densities.

6. DISCUSSION

Among all three of the compositions tested, 85:15 wt-% V_2O_5:B_2O_3 glass had the best electrochemical performance. This material has the highest initial specific capacity, 222 mAh/g, highest capacity retention at 100 cycles, 64%, and recovered most of the capacity when cycled with varying current densities. 80:20 wt-% V_2O_5:B_2O_3 glass was the second-best composition with initial specific capacity value of 207 mAh/g, 60% capacity retention and relatively worse rate capability. 90:10 wt-% V_2O_5:B_2O_3 glass performed the worst with 191 mAh/g initial capacity, 53% capacity retention and rate capability.

The relatively worse electrochemical performance of the 90:10 wt-% V_2O_5:B_2O_3 glass can be explained with formation of heterogeneous samples caused by increased V_2O_5 concentration, which can be seen in SEM images of the sample. Considering the 80:20 and 85:15 wt-% V_2O_5:B_2O_3 glass, V_2O_5 concentration does not affect the performance negatively, on the contrary better electrochemical performance of the 85:15 wt-% V_2O_5:B_2O_3 glass can be explained by increased V_2O_5 concentration.

According to all these results, the proposed V_2O_5:B_2O_3 glass material with proper ratios successfully increased the electrochemical performance of the V_2O_5 when used as a cathode material in lithium-ion batteries.

7. FUTURE WORKS

In this study, V_2O_5-B_2O_3 glassy material is synthesized. According to XRD patterns the synthesized material is not in pure glass form. Improving the synthesis method to acquire an amorphous structure could further benefit the electrochemical characteristics of the material. Optimizing the ratio between V_2O_5 and B_2O_3 should be investigated.

Apart from rGO, other additives should be investigated. Overall performance of the material could further be improved with better electrode engineering.

REFERENCES

[1] Tarascon J.M., Armand M., (2001), "Issues and Challenges Facing Rechargeable Lithium Batteries.", Nature, 414, 359–367.

[2] Afyon S., Krumeich F., Mensing, C.Borgschulte A., Nesper R., (2014), "New High Capacity Cathode Materials for Rechargeable Li-ion Batteries: Vanadate-Borate Glasses.", Scientific Reports, 4, 7113.

[3] Rui X., Zhu J., Sim D., Xu C., Zeng Y., Hng, H. H., Lim T. M., Yan Q., (2011), "Reduced Graphene Oxide Supported Highly Porous V_2O_5 Spheres as a High-Power Cathode Material for Lithium İon Batteries.", Nanoscale, 3 (11), 4752–4758.

[4] Dixit A., (2020), "Cathode Materials for Lithium Ion Batteries (LIBs): A Review on Materials related aspects towards High Energy Density LIBs.", SMC Bulletin, 10 (3).

[5] Verma P., Maire P., Novák P., (2010), "A Review of the Features And Analyses of the Solid Electrolyte Interphase In Li-ion Batteries.", Electrochimica Acta, 55 (22), 6332–6341.

[6] Deng D., (2015), "Li-ion Batteries: Basics, Progress, and Challenges.", Energy Science and Engineering, 3 (5), 385–418.

[7] Liu C., Li F., Lai-Peng M., Cheng H. M., (2010), "Advanced Materials for Energy Storage.", Advanced Materials, 22 (8), 28–62.

[8] Wakihara M., (2001), "Recent Developments in Lithium Ion Batteries.", Materials Science and Engineering: R: Reports, 33 (4), 109–134.

[9] Zheng J., Myeong S., Cho W., Yan P., Xiao J, Wang C., Cho J., Zhang J., (2017), "Li and Mn-Rich Cathode Materials: Challenges to Commercialization.", Advanced Energy Materials, 7 (6).

[10] Radin M. D., Hy S., Sina M., Fang C., Liu H., Vinckeviciute J., Zhang M., Whittingham M. S., Meng Y. S., Van der Ven A., (2017), "Narrowing the Gap Between Theoretical and Practical Capacities in Li-Ion Layered Oxide Cathode Materials.", Advanced Energy Materials, 7 (20), 1–33.

[11] Manthiram A., (2020), "A Reflection on Lithium-ion Battery Cathode Chemistry.", Nature Communications, 11 (1), 1–9.

[12] Whittingham M. S., (2004), "Lithium Batteries and Cathode Materials.", Chemical Reviews, 104 (10), 4271–4301.

[13] Xia H., Meng Y. S., Lu L., Ceder, G., (2007), “Electrochemical Behavior and Li Diffusion Study of $LiCoO_2$ Thin Film Electrodes Prepared by PLD.”, Scientific Commons.

[14] Schipper F., Aurbach D., (2016), “A Brief Review: Past, Present and Future of Lithium Ion Batteries.”, Russian Journal of Electrochemistry, 52 (12), 1095–1121.

[15] Myung S. T., Maglia F., Park K. J., Yoon C. S., Lamp P., Kim S. J., Sun Y., (2017), “Nickel-Rich Layered Cathode Materials for Automotive Lithium-Ion Batteries: Achievements and Perspectives.”, ACS Energy Letters, 2 (1), 196–223.

[16] Liu W., Oh P., Liu X., Lee M. J., Cho W., Chae S., Kim Y., Cho J., (2015), “Nickel-Rich Layered Lithium Transition-Metal Oxide for High-Energy Lithium-Ion Batteries.”, Angewandte Chemie - International Edition, 54 (15), 4440–4457.

[17] Fergus J. W., (2010), “Recent Developments in Cathode Materials for Lithium Ion Batteries.”, Journal of Power Sources, 195 (4), 939–954.

[18] Huang Y., Dong Y., Li S., Lee J., Wang C., Zhu Z., Xue W., Li Y., Li J., (2021), “Lithium Manganese Spinel Cathodes for Lithium-Ion Batteries.”, Advanced Energy Materials, 11 (2), 1–21.

[19] House R. A., Bruce P. G., (2020), “Lightning Fast Conduction.”, Nature Energy, 5 (3), 191–192.

[20] Tolganbek N., Yerkinbekova Y., Kalybekkyzy S., Bakenov Z., Mentbayeva A., (2021), “Current State of High Voltage Olivine Structured $LiMPo_4$ Cathode Materials for Energy Storage Applications: A Review.”, Journal of Alloys and Compounds, 882.

[21] Yamada A., Chung S. C., Hinokuma K., (2001), “Optimized $LiFePO_4$ for Lithium Battery Cathodes.”, Journal of The Electrochemical Society, 148 (3).

[22] Sgroi M. F., Lazzaroni R., Beljonne D., Pullini D., (2017), “Doping $LiMnPo_4$ with Cobalt and Nickel: A first Principle Study.”, Batteries, 3 (2).

[23] Wu Y. P., Rahm E., Holze R., (2003), “Carbon Anode Materials for Lithium Ion Batteries.”, Journal of Power Sources, 114 (2), 228-336.

[24] Sandhya C. P., John B., Gouri C., (2014), “Lithium Titanate as Anode Material for Lithium-Ion Cells: A Review.” Ionics, 20 (5), 601–620.

[25] Zhang W. J., (2011), “A Review of the Electrochemical Performance of Alloy Anodes for Lithium-Ion Batteries.”, Journal of Power Sources, 196 (1). 13–24.

[26] Zhang S. S., (2006), “A Review on Electrolyte Additives for Lithium-Ion Batteries.”, Journal of Power Sources, 162 (2 SPEC. ISS.), 1379–1394.

[27] Meyer W. H., (1998), “Polymer Electrolytes for Lithium-Ion Batteries.”, Advanced Materials, 10 (6), 439-448.

[28] Stephan A. M., (2006), “Review on Gel Polymer Electrolytes for Lithium Batteries.”, European Polymer Journal, 42 (1). 21–42.

[29] Li J., Daniel C., Wood D., (2011), “Materials Processing for Lithium-Ion Batteries”, Journal of Power Sources, 196 (5), 2452-2460.

[30] Arora P., Zhang Z., (2004), “Battery Separators.”, Chemical Reviews, 104 (10), 4419–4462.

[31] Zhou Y. Y., Zhang Z. Y., Zhang H. Z., Li, Y., Weng Y., (2021), “Progress and Perspective of Vanadium-Based Cathode Materials for Lithium Ion Batteries.”, Tungsten, 3 (3), 279–288.

[32] Li Y., Ji S., Gao Y., Luo H., Kanehira M., (2013), “Core-shell VO_2 @TiO_2 Nanorods that Combine Thermochromic and Photocatalytic Properties for Application ss Energy-Saving Smart Coatings.”, Scientific Reports, 3, 1–13.

[33] Mai L., Wei Q., An Q., Tian X., Zhao Y., Xu X., Xu L., Chang L., Zhang Q., (2013), “Nanoscroll Buffered Hybrid Nanostructural VO_2(B) Cathodes for High-Rate and Long-Life Lithium Storage.”, Advanced Materials, 25 (21), 2969–2973.

[34] Niu C., Meng J., Han C., Zhao K., Yan M., Mai L., (2014), “VO_2 Nanowires Assembled Into Hollow Microspheres for High-Rate and Long-Life Lithium Batteries.”, Nano Letters, 14 (5), 2873–2878.

[35] Yu Q., Qian Y., Zhang L., Wang X., Li X., (2015), “Synthesis and Electrochemical Performance of Ni-Doped VO_2(B) as a Cathode Material for Lithium Ion Batteries.”, Cailiao Kexue yu Gongyi/Material Science and Technology, 23 (6), 29–33.

[36] Wadsley A. D., (1957), “Crystal Chemistry of Non-stoichiometric Pentavalent Vanadium Oxides: Crystal Structure of Li1+XV3O8.”, Acta Crystallographica, 10, 261-267.

[37] Tan H. T., Rui X., Sun W., Yan Q., Lim T. M., (2015), “Vanadium-Based Nanostructure Materials for Secondary Lithium Battery Applications.”, Nanoscale, 7 (35), 14595–14607.

[38] Mei P., Wu X. L., Xie H., Sun L., Zeng Y., Zhang J., Tai L., Guo X., Cong L., Ma S., Yao C., Wang R., (2014), “LiV_3O_8 Nanorods as Cathode Materials for High-Power and Long-Life Rechargeable Lithium-Ion Batteries.”, RSC Advances, 4 (49), 25494–25501.

[39] Song H., Liu Y., Zhang C., Liu C., Cao G., (2015), "Mo-doped LiV_3O_8 Nanorod-Assembled Nanosheets as a High Performance Cathode Material for Lithium Ion Batteries.", Journal of Materials Chemistry A, 3 (7), 3547–3558.

[40] Gaubicher J., Wurm C., Goward G., Masquelier C., Nazar L., (2000), "Rhombohedral Form of $Li_3V_2(PO_4)_3$ as a Cathode in Li-ion Batteries.", Chemistry of Materials, 12 (11), 3240–3242.

[41] Tan H., Xu L., Geng H., Rui X., Li C., Huang S., (2018), "Nanostructured $Li_3V_2(PO_4)_3$ Cathodes.", Small, 14 (21), 1–22.

[42] Fei L., Sun L., Lu W., Guo M., Huang H., Wang J., Chan H., Fan S., Wang Y., (2014), "Stable 4 V-Class Bicontinuous Cathode by Hierarchically Porous Carbon Coating on $Li_3V_2(PO_4)_3$ Nanospheres.", Nanoscale, 6, 12426–12433.

[43] Zeng X. X., Chen H., Guo G., Li S. Y., Liu J. Y., Ma Q., Liu G., Yin Y., Wu X., Guo Y., (2020), "Raising the Capacity of Lithium Vanadium Phosphate via Anion and Cation Co-Substitution.", Science China Chemistry, 63 (2), 203–207.

[44] Zhong S., Zhang X., Liu J., Sui Y., (2020), "Study on $xLiVPO_4F \cdot yLi_3V_2(PO_4)_3$/C Composite for High-Performance Cathode Material for Lithium-Ion Batteries.", Frontiers in Chemistry, 8, 1–9.

[45] Yang Y., Li L., Fei H., Peng Z., Ruan G., Tour J. M., (2014), "Graphene Nanoribbon/V_2O_5 Cathodes in Lithium-ion Batteries.", ACS Applied Materials and Interfaces, 6 (12), 9590–9594.

[46] Delmas C., Cognac-Auradou H., Cocciantelli J., Ménétrier M. M., Doumerc J. P., (1994), "The $Li_xV_2O_5$ System: An Overview of the Structure Modifications Induced by the Lithium Intercalation," Solid State Ionics, 69 (3–4), 257–264.

[47] Cocciantelli J., Ménétrier M. M., Delmas C., Doumerc J. P., Pouchard M., Broussely M., Labat J., (1995), "On the $\delta \rightarrow \gamma$ Irreversible Transformation in Li//V_2O_5 Secondary Batteries.", Solid State Ionics, 78 (1–2), 143-150.

[48] Yu D., Chen C., Xie S., Liu Y., Park K., Zhou X., Zhang Q., Li J., Cao G., (2011), "Mesoporous Vanadium Pentoxide Nanofibers with Significantly Enhanced Li-Ion Storage Properties by Electrospinning.", Energy and Environmental Science, 4 (3), 858–861.

[49] Mai L., Xu L., Han C., Xu X., Luo Y., Zhao S., Zhao Y., (2010), "Electrospun Ultralong Hierarchical Vanadium Oxide Nanowires with High Performance for Lithium Ion Batteries.", Nano Letters, 10 (11), 4750–4755.

[50] Rui X., Zhu J., Liu W., Tan H., Sim D., Xu C., Zhang H., Ma J., Hng H. H., Lim T. M., Yan Q., (2011), "Facile Preparation of Hydrated Vanadium Pentoxide Nanobelts Based Bulky Paper as Flexible Binder-Free Cathodes for High-Performance Lithium Ion Batteries.", RSC Advances, 1 (1), 117–122.

[51] Li Y., Yao J., Uchaker E., Yang J., Huang Y., Zhang M., Cao G., (2013), "Leaf-Like V_2O_5 Nanosheets Fabricated by a Facile Green Approach as High Energy

Cathode Material for Lithium-Ion Batteries.", Advanced Energy Materials, 3 (9), 1171.

[52] Wang Y., Zhang H. J., Lim W. X., Lin J. Y., Wong C. C., (2011), "Designed Strategy to Fabricate a Patterned V_2O_5 Nanobelt Array as a Superior Electrode for Li-Ion Batteries.", Journal of Materials Chemistry, 21 (7), 2362–2368.

[53] Rui X., Lu Z., Yu H., Yang D., Hng H. H., Lim T. M., Yan Q., (2013), "Ultrathin V_2O_5 Nanosheet Cathodes: Realizing Ultrafast Reversible Lithium Storage.", Nanoscale, 5 (2), 556–560.

[54] Li Y., Yao J., Uchaker E., Zhang M., Tian J., Liu X., Cao G., (2013), "Sn-doped V_2O_5 Film with Enhanced Lithium-Ion Storage Performance.", Journal of Physical Chemistry C, 117 (45), 23507–23514.

[55] Yu D. M., Zhang S. T., Liu D. W., Zhou X. Y., Xie S. H., Zhang Q. F., Liu Y. Y., Cao G. Z., (2010) "Effect of Manganese Doping on Li-Ion İntercalation Properties of V_2O_5 Films.", Journal of Materials Chemistry, 20 (48), 10841–10846.

[56] Yu H., Rui X., Tan H., Chen J., Huang X., Xu C., Liu W., Yu D. Y. W., Hng H. H., Hoster H. E., Yan Q., (2013), "Cu Doped V_2O_5 Flowers as Cathode Material for High-Performance Lithium Ion Batteries.", Nanoscale, 5 (11), 4937–4943.

[57] Zhan S. Y., Wang C. Z., Nikolowski K., Ehrenberg H., Chen G., Wei Y. J., (2009), "Electrochemical Properties of Cr Doped V_2O_5 Between 3.8 V and 2.0 V", Solid State Ionics, 180 (20–22), 1198–1203.

[58] Saetova N. S., Raskovalov A. A., Antonov B. D., Denisova T. A., Zhuravlev N. A., (2020), "Structural Features of $Li_2O–V_2O_5–B_2O_3$ Glasses: Experiment and Molecular Dynamics Simulation.", Journal of Non-Crystalline Solids, 545.

[59] Liao J., Ye Z., (2018), "Nontrivial Effects of 'Trivial' Parameters on the Performance of Lithium–Sulfur Batteries.", Batteries, 4 (2), 22.

BIOGRAPHY

In 2013, Mehmet Sinan Uyanık graduated from Burak Bora Anatolian High School and started to study for his bachelor's degree in mechanical engineering in Dokuz Eylül University. After graduating, he started to study for his master's degree in mechanical engineering in Gebze Technical University in 2020. He has been working as a research assistant in Gebze Technical University Institute of Energy Technologies since February 2021.